Volume 4
Number 2
February 2024
Pages 107–284

Environmental Science
Atmospheres

rsc.li/esatmospheres

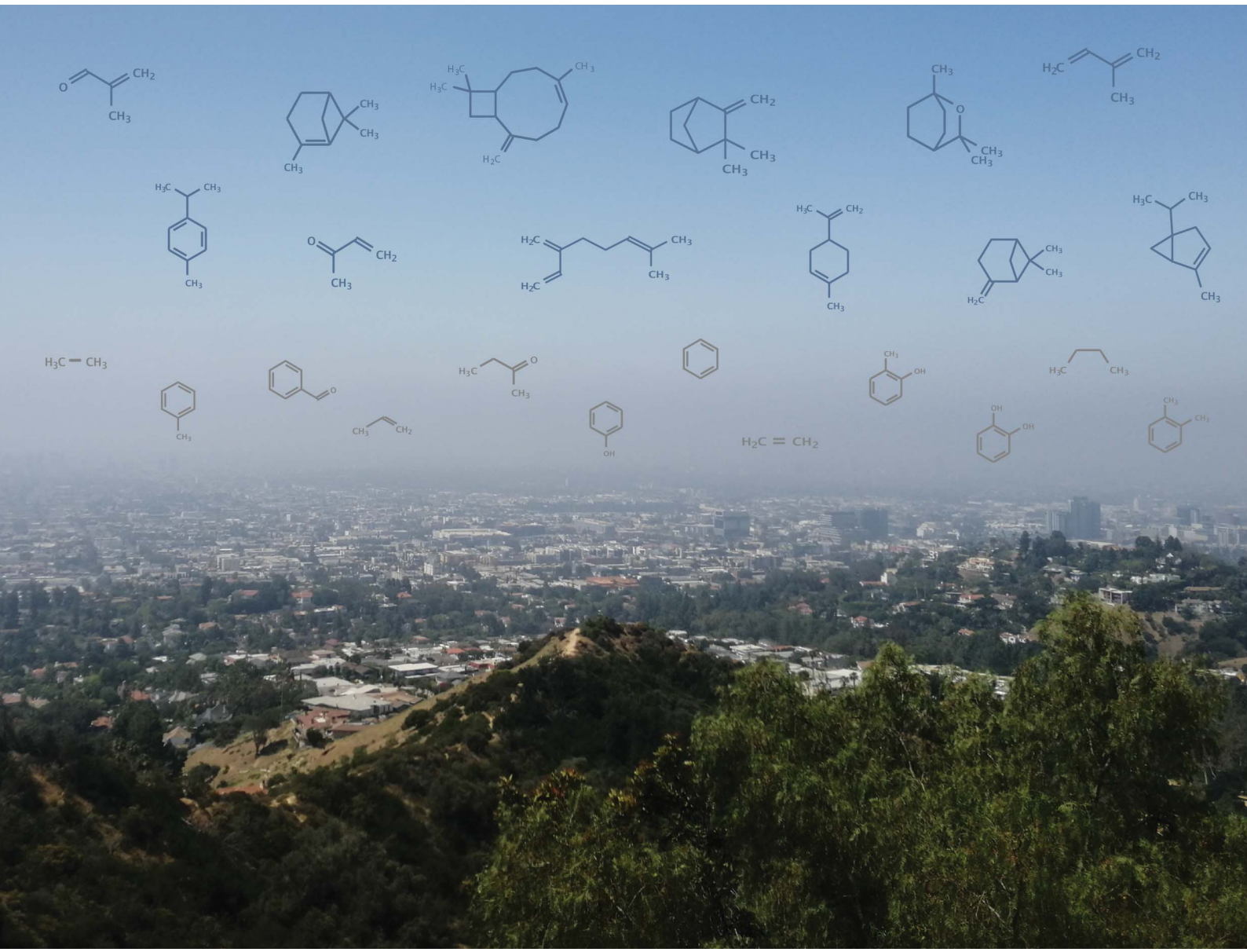

ISSN 2634-3606

ROYAL SOCIETY OF CHEMISTRY

PAPER

Marie Luise Luttkus *et al.*
Urban and Remote cheMistry modELLing with the new chemical mechanism URMELL: part I gas-phase mechanism development

Environmental Science: Atmospheres

ROYAL SOCIETY OF CHEMISTRY

PAPER

View Article Online
View Journal | View Issue

Cite this: *Environ. Sci.: Atmos.*, 2024, **4**, 164

Urban and Remote cheMistry modELLing with the new chemical mechanism URMELL: part I gas-phase mechanism development†

Marie Luise Luttkus, *[a] Erik Hans Hoffmann, [b] Andreas Tilgner, [b] Ralf Wolke, [a] Hartmut Herrmann [b] and Ina Tegen [a]

Air quality is a globally pressing issue as it poses a major threat for human health and ecosystems. Non-methane volatile organic compounds (NMVOCs) are highly reactive substances and known for their impact on O_3, HO_x (OH + HO_2) and NO_x (NO + NO_2) concentrations. NMVOCs comprise a variety of anthropogenic and biogenic compounds with highly complex and entangled relations. Therefore, it is key to capture these interdependencies for any air quality assessment through modeling. Unfortunately, chemical mechanisms used for air quality modeling are often too simplified and partly outdated. Here, we present the development of the chemical mechanism URMELL (Urban and Remote cheMistry modELLing) comprising an extended chemical treatment of major anthropogenic and biogenic NMVOCs based on current knowledge. Box model simulations of standardized urban and remote conditions were performed with URMELL and other mechanisms, and the obtained concentration time profiles of key compounds were compared. High correlations (>0.9) with the benchmark mechanism MCMv3.3.1 are found for all urban conditions. For remote conditions, the simulations using URMELL have much higher oxidant concentrations, especially for OH reaching concentrations ~10^6 molecules per cm^3 which is in the same range of measured ambient OH concentrations at remote isoprene-dominated sites. For further evaluation, URMELL was applied in the chemical transport model COSMO-MUSCAT and simulations for Germany in May 2014 were performed. Modeled O_3, NO and NO_2 concentrations were compared with 57 measurement sites indicating improved ozone correlations for urban as well as remote isoprene-influenced sites than the currently applied mechanism.

Received 23rd June 2023
Accepted 18th December 2023

DOI: 10.1039/d3ea00094j

rsc.li/esatmospheres

Environmental significance

The chemical degradation of anthropogenic and biogenic NMVOCs differs significantly implying individual impacts on air pollutants. Future emission regulations will lead to a decline of anthropogenic sources whereas biogenic sources will increase, due to climate warming and climate mitigation strategies such as tree planting programs. Therefore, the importance of biogenic NMVOCs such as isoprene with respect to air quality measures will increase and will require a more comprehensive treatment in chemical transport models than is currently the case. To this aim, a gas-phase chemistry mechanism for regional CTMs was developed with extended treatment for key biogenic and anthropogenic NMVOCs. This study highlights specific important adjustments through sensitivity studies and quantifies the significant increases in isoprene-dominated remote OH and O_3 concentrations.

1 Introduction

Non-methane volatile organic compounds (NMVOCs) are emitted into the troposphere by various anthropogenic (AVOC) and biogenic (BVOC) sources. Once emitted, they initiate complex chemical and photochemical degradation chains impacting tropospheric chemistry and thus the gas- as well as particle-phase composition. The multistep oxidation of NMVOCs therefore, impacts regional air quality[1–4] on a short term and the climate[5,6] on a larger timescale. NMVOC oxidation is coupled with the NO_x (NO_x = NO + NO_2) and HO_x (HO_x = OH + HO_2) budget and thus affects both directly and/or indirectly O_3

[a]*Department Modeling of Atmospheric Processes, Leibniz Institute for Tropospheric Research (TROPOS), Permoserstr. 15, 04318 Leipzig, Germany. E-mail: luttkus@tropos.de*

[b]*Atmospheric Chemistry Department (ACD), Leibniz Institute for Tropospheric Research (TROPOS), Permoserstr. 15, 04318 Leipzig, Germany*

† Electronic supplementary information (ESI) available: URMELL species list, complex rate coefficients, chemical and photolysis reactions, additional information about box and CTM model simulation with SPACCIM and COSMO-MUSCAT including figures and statistics. See DOI: https://doi.org/10.1039/d3ea00094j

as well as secondary organic aerosol (SOA) formation.[4,7–10] As SOA formation can significantly impact the aerosol particle number, mass concentration and chemical composition, NMVOC oxidation affects the physico-chemical properties of clouds and thus cloud and precipitation formation processes.[6,11–17]

Moreover, the oxidation of NMVOCs impacts the atmospheric oxidizing capacity, especially the OH concentration. This has major effects on the lifetime of numerous other trace gases including SO_2, CO and the greenhouse gas methane which all favor OH as reaction partner. However, the extent of NMVOC chemistry induced perturbations depend on the atmospheric environment in which the oxidation occurs. Accordingly, different impacts have to be expected for clean rural and polluted urban/industrialized areas.[18–21] Progressing NMVOC oxidation leads to the production of highly oxidized products with multifunctional groups: under high NO_x conditions, organic nitrates can form,[22,23] while in cleaner environments, products with multiple hydroperoxy (OOH), carbonyl (C=O) and/or hydroxy (OH) groups form.[24,25] The formation of organic nitrates, in particular PAN, can be an important NO_x reservoir on the one hand decreasing NO_x concentrations in a certain area. On the other hand, due to atmospheric transport and decomposition processes, PANs can increase NO_x concentrations in other less polluted areas. Under low NO_x conditions, the same holds for highly oxidized organic molecules (HOMs) which affect the HO_x budget equally. But, in contrast to PANs, HOMs are important SOA sources.

The majority of NMVOCs are BVOCs emitted from plants.[6,26] Globally, the most abundant BVOC is isoprene (C_5H_8) with estimated 535 Tg per year.[26] Therefore, CTMs have to describe its chemistry accurately, even if only treating parameterized reaction sequences. Otherwise the CTMs can fail to predict concentrations of adjunct chemical systems. During the last decades, a discrepancy between modeled and measured HO_x concentration was identified in remote isoprene-rich environments.[9,10,28] Thus, a lot of efforts have been made to improve our knowledge of isoprene chemistry and to adapt the applied gas-phase chemistry mechanisms.[9,10,27–30]

To capture BVOC effects on the gas- and particle-composition of the troposphere also mono- and sesquiterpene chemistry have to be described adequately, too. Sesquiterpenes account for about 3% (29 Tg per year) of total BVOC emissions and therefore only play a minor role.[26] For β-caryophyllene, the most abundant sesquiterpene, a reduced mechanism has been published by Khan *et al.*[31] including the determination of SOA precursor substances. Monoterpenes account for about 20% (162 Tg per year) of global BVOC emissions,[26] but are highly plant species-specific and thus depend on vegetation cover. Their influence on atmospheric chemistry intensifies poleward, as coniferous forests emit less isoprene but higher quantities of monoterpenes. The principal NO_x/O_3 interrelations are similar to isoprene while the final ozone forming potentials differ.[32–34] Moreover, monoterpenes have a higher SOA formation potential and dominate the SOA composition in coniferous forests.[12,35,36] So far, only a few lumped monoterpene species are currently included in chemical mechanisms of CTMs.[37–43] Recent research suggests, that even within these lumped clusters the SOA forming potential can vary significantly between different monoterpenes.[24,25,44–48] However, as this is still an open research field and new findings emerge frequently, the present study mainly remains focused on the most abundant BVOC isoprene.

Considering the fact that most people live in cities and the number of city dwellers is still climbing, anthropogenic emission sources are also of key importance, especially in terms of urban air quality. Cities face new challenges in the near future of yet unknown consequences, due to air quality measures, climate change and mitigation strategies. In urban areas, air quality measures such as changes in the car fleet will decrease NO_x and AVOC emissions in the future. At the same time an increase in urban green infrastructure is favored by urban development planning due to climate mitigation measures. Thus, urban environments will likely undergo a shift from AVOC to BVOC emissions. Thereby, urban green infrastructure strategies rest on planting trees. Importantly, the tree species-specific BVOC emissions are additionally impacted by stressors such as heat and drought.[49–53] Overall, cities will undergo a change in the near future making it more challenging to determine the sources of air pollutants such as O_3 and particular matter (PM), because of growing NMVOC diversity. Hence, as O_3, NO_x and PM impact the human health and the ecosystem it is of utmost importance to cover a wide variety of VOCs along with their $HO_x/NO_x/O_3$/SOA interdependencies in CTMs typically used for air quality assessments.

Numerous chemical gas-phase mechanisms with varying complexity are currently available. The most detailed one is the MCM3.3.1,[54–59] but due to its high complexity it is not directly applicable in CTMs. Nevertheless, the MCM is often used as reference mechanism when mechanisms with reduced complexity are developed. In CTMs, these condensed mechanisms are favored due to their smaller amount of substances and reactions while remaining a sufficient accuracy and minimizing the computation time. Commonly used CTM mechanisms are: RACM,[37] RACM2,[38] JAM,[39] MOZART,[40] the carbon bond mechanism[41] and SAPRC.[42,43] While all these mechanisms focus on NO_x/O_3 predictability, the formation of higher oxidized molecules is not described sufficiently enough to enable the inclusion of direct SOA formation. Instead gas-phase chemistry and SOA formation are treated separately, if considered at all.

Next to the chemical mechanism, an accurate description of emission fields is mandatory including vegetative/natural and manmade emissions. This will ensure adequate anthropogenic and biogenic interactions from the origin, processing throughout the transport to the deposition.

To date, the currently applied mechanisms in and emission setups of CTMs are not capable to project these problems sufficiently, because of issues related to complexity of chemistry mechanisms and deposition schemes, as well as adequate input data such as the description of emission and meteorological fields *etc.* In order to address these issues, we developed a more complex biogenic emission scheme to capture tree species-specific BVOC emissions within the CTM COSMO-MUSCAT in a previous study.[4] As a next step, we developed and applied the new chemistry mechanism URMELL (Urban and Remote

cheMistry modELLing), which is presented in this study. URMELL combines recent knowledge of both anthropogenic (*e.g.* aromatic chemistry) and biogenic (*e.g.* isoprene chemistry) organic compounds. We present multiple comparisons of various sensitivity box model and CTM simulations that reveal the appropriateness of URMELL for air quality modelling.

2 Mechanism developments

The basis for the URMELL mechanism development is the chemical mechanism JAM version 002b[39] applied in the global chemistry-climate model ECHAM6.3-HAM2.3-MOZ1.0. This mechanism is further denoted JAMv2b. JAMv2b is based on the Model of Ozone and Related Tracers (MOZART) v.4 for tropospheric and the Whole Atmosphere Chemistry Climate Model (WACCM) for stratospheric chemistry.[40,60] Additionally, Jamv2b also includes a more detailed representation of isoprene by integrating the Mainz Isoprene Mechanisms 2 (MIM-2),[29] 1,6 H-shift reactions,[27] epoxide formation[61] and HPALD photolysis.[62] Further information about JAMv2b[39] can be found in the corresponding publication. Compared to other mechanisms available at the time of publication and initial URMELL mechanism development, JAMv2b is more detailed and treats a larger number of species explicitly whereby reducing the number of lumped species and featuring newer measurement results.

So far, RACM-MIM2-ext[4,37,63] had been used for air quality assessments in the model framework COSMO-MUSCAT at TROPOS.[64–66] Advantageously, the JAMv2b mechanism already contains a more up-to-date chemistry implementation compared to RACM.[37,39] However, within the last five years since JAMv2b was published, new findings from laboratory experiments emerged. In order to take them into account, the reactions within this mechanism have been first screened to include the latest recommendations of kinetic reaction rate constants and oxidation products (see Sect. 2.1–2.5 for further details).

However, the major focus of the mechanism development described here has been put on the integration of possible SOA precursor compounds to enable a direct and more explicit SOA approach. Therefore, already existing reaction pathways have been investigated to identify possible reaction chains leading to highly functionalized products with low volatility that are currently not included in JAMv2b. As URMELL is intended to be applied for air quality assessments considering both anthropogenic and biogenic sources for air pollutants, these SOA extensions are considered for their main contributors: aromatics (Sect. 2.4) and isoprene (Sect. 2.5). Here, the focus is on aromatics and isoprene, as a lot of effort has already been made to determine their chemical degradation schemes.

All in all, this study focuses on aromatics and isoprene chemistry updates and extensions leading to an advanced gas-phase mechanism. Finally, this mechanism development aims at a more sophisticated Urban and Remote cheMistry modELLing, from which the designation of the new mechanism URMELL was derived. Species number and complexity was increased substantially by maintaining possible gas-phase SOA compounds in order to enable an explicit SOA formation implementation. Overall, URMELL contains 313 species (listed in Table S1-1†), and 916 reactions (summarized in Tables S1-2 and S1-3†). In Table S1-1,† new species are presented in bold font and new and/or changed reactions in Tables S1-2 and S1-3† are marked in a separate column. The most important changes to JAMv2b are summarized in the following subsections (2.1–2.5). Note while all the described changes apply to JAMv2b, some of the updates might already be considered in other mechanisms to some extent. After a positive follow-up feasibility study in terms of explicit SOA modeling, URMELL will be extended to monoterpenes where feasible, too.

2.1 Important general modifications in URMELL

In the following, a brief description of the most important general modifications in URMELL is provided. All reactions of JAMv2b were first screened to include more recent recommendations of kinetic reaction rate constants as well as oxidation products and photolysis rates, *e.g.* by using either the database of the IUPAC task group on atmospheric chemical kinetic data evaluation (**https://iupac.aeris-data.fr/en/home/**)[67–74] or the near explicit master chemical mechanism (MCM3.3.1; **http://mcm.york.ac.uk/**).[54–59] These updates already affect the simple O_x, HO_x and NO_x chemistry, as well as smaller organic compounds such as glyoxal (GLY), methylglyoxal (MGLY) or methyl ethyl ketone (MEK).

2.1.1 Smaller organic compounds chemistry. The oxidation chemistry of MEK in JAMv2b is mainly based on $MEKBO_2$, but according to MCM3.3.1, $MEKAO_2$ accounts for 45.9%, $MEKBO_2$ for 46.2%, and $MEKCO_2$ for 7.9%. IUPAC recommends a ratio of 62% for $MEKBO_2$. The structure–activity relationship (SAR) method yields roughly 33%/57%/10%, respectively at 298 K.[75] Here we use the 62% yield for $MEKBO_2$ and scale the yields for $MEKAO_2$ (29.4%) and $MEKCO_2$ (8.6%) accordingly to the SAR method. For the reaction of $MEKCO_2$ with CH_3O_2 and $CH_3C(O)O_2$, the same IUPAC recommendations as for propyldioxy, another organic peroxy radical with a neighboring carbonyl group, is applied as there is no individual data available. Another significant change was made for the reaction rate constant of GLY with NO_3. In most mechanisms, the reaction rate constant of acetaldehyde has been used for this reaction so far. However, there is a preferred value of 4×10^{-16} cm^3 per molecules per s available (IUPAC) which is about four orders of magnitudes lower than in JAMv2b[39] (2.5×10^{-12} cm^3 per molecules per s) and still one order of magnitude lower than the reaction rate constant (k_{NO_3AL} based on acetaldehyde) used in MCM3.3.1, MAGRITTE[76] and MIM2.[29] Also, the rate coefficient for peracetic acid changed by two orders of magnitudes from 3.7×10^{-12} (MCM3.3.1) to 3×10^{-14} cm^3 per molecules per s (IUPAC). For substances with no IUPAC recommendation the reaction rate coefficient and ratios have been calculated using the SAR method,[75] if appropriate.

2.1.2 Sesquiterpenes chemistry. Additionally, the chemistry of sesquiterpenes, represented by β-caryophyllene, was updated using the mechanism described by Khan *et al.*[31] After two oxidation steps, sesquiterpene chemistry merges into the CRI α-pinene scheme. Therefore, progressing degradation leads to the formation of lumped monoterpene (a C10 and a C5)

reaction products. These products are not directly included in URMELL yet and are lumped into TERP2O_2 and CO_2C_3CHO, respectively. Further adjustments were done to P1OOH (sesquiterpene HOM product) due to lower established volatility of this sesquiterpene HOM compared to Khan *et al.*[31] turning it into a non-volatile product. Therefore, P1OOH is considered to transfer entirely into the particle-phase, analogue to P2OOH and P2NO3, neglecting its gas-phase reaction pathways.

2.2 Ozonolysis implementation updates

Besides the OH-radical oxidations, the ozonolysis reaction schemes of ethene and propene are updated using the recent IUPAC task group recommendations by Cox *et al.*[73] The ozonolysis of ethene (R-1) and (R-2) yields formaldehyde and the exited Criegee intermediate [CH_2OO]* which yields the stable Criegee intermediate CH_2OO. Further details on CH_2OO chemistry are given in the next section (Sect. 2.3). As for the MCM3.3.1, in URMELL the reaction products HCO and H of (R-2) are considered to immediately react with O_2 and turn into CO + HO_2 (JPL) and HO_2, respectively.

$$C_2H_4 + O_3 \rightarrow HCHO + [CH_2OO]^* \quad \text{(R-1)}$$

$$[CH_2OO]^* \rightarrow 0.17(OH + HCO) + 0.18(CO + H_2O) + 0.23CO_2 + 0.18H_2 + 0.1H + 0.42CH_2OO \quad \text{(R-2)}$$

The ozonolysis of propene (R-3) yields acetaldehyde (CH_3CHO), [CH_2OO]*, formaldehyde and two excited Criegee intermediates [*E*-CH_3CHOO]* and [*Z*-CH_3CHOO]* which both can be transferred into stabilized Criegee intermediates *E*-CH_3CHOO and *Z*-CH_3CHOO. For the latter one, thermal decomposition is expected to be the dominating pathway releasing OH and CH_2CHO, which oxidation by O_2 leads to $OOCH_2CHO$. Following the main reaction pathway of $HCOCH_2O_2$ (MCM3.3.1), $OOCH_2CHO$ becomes HCHO + HO_2 + CO. About 60% of [*E*-CH_3CHOO]* decomposes yielding CH_4, CO_2, CH_3OH, CO, CH_2CO and H_2O. Subsequent oxidation of CH_2CO by OH and O_2 (IUPAC) produces CO + HCHO + HO_2.[77] The remaining 40% form the stabilized Criegee intermediate *E*-CH_3CHOO.

$$C_3H_6 + O_3 \rightarrow 0.38CH_3CHO + 0.38[CH_2OO]^* + 0.62HCHO + 0.32[E\text{-}CH_3CHOO]^* + 0.3[Z\text{-}CH_3CHOO]^* \quad \text{(R-3)}$$

Within the next section, the chemistry of the stabilized Criegee intermediates CH_2OO and *E*-CH_3CHOO are addressed further. Note, that in Jamv2b the reaction of C_3H_6 with O_3 has a direct CH_3O_2 production channel and the MCM3.3.1 also produces CH_3O_2 through the exited Criegee intermediate (CH_3CHOOA) channel.

2.2.1 Chemistry of the stabilized Criegee intermediate CH_2OO. In URMELL, CH_2OO is formed through the ozonolysis of ethene,[73] propene,[73] isoprene,[30] MACR and MVK.[30] Additionally, the reaction of CH_3O_2 with OH yields 0.05 CH_2OO (IUPAC).

Based on the IUPAC recommendations, the chemical degradation of CH_2OO under tropospheric conditions is dominated by the reaction with the water dimer.[73] Unfortunately, the two laboratory studies from Sheps *et al.*[78] (ratios presented in bold) and Nguyen *et al.*[79] (ratios given in brackets) provide inconsistent results regarding the branching ratios of the reaction pathways (R-4):

$$CH_2OO + (H_2O)_2 \rightarrow \begin{cases} \mathbf{0.55}\ (0.4) \times (HOCH_2OOH + H_2O) \\ \mathbf{0.4}(0.06) \times (HCHO + H_2O_2 + H_2O) \\ \mathbf{0.05}\ (0.54) \times (HCOOH + 2H_2O) \end{cases} \quad \text{(R-4)}$$

Both studies report comparable branching ratios for (R-4) of 0.55 and 0.4, respectively. However, the contributions to (R-4) (0.4 and 0.06) and (R-4) (0.05 and 0.54) are very different. This generates uneven production strengths for formaldehyde (HCHO) and formic acid (HCOOH). Recent studies revealed that potential chemical sources of HCOOH are missing in up-to-date mechanisms.[80–82] Therefore, the formation pathways of HCOOH are in the focus of current research, because of its importance for future evolvement of atmospheric acidity. But no recommendations have been done so far for (R-4).[73] Therefore, after the main mechanism development was finished, first evaluation simulations were performed (see S2.1 for details). In these sensitivity simulations, either the yields of Nguyen *et al.*[79] or the yields from Sheps *et al.*[78] are applied to examine their effect on the gas-phase compositions predicted by URMELL (see Fig. 2). The sensitivity studies reveal a significant impact on gas-phase HCOOH production. Therefore, it is important to further clarify the branching ratios for this reaction. This would also help to quantify the discrepancies between measured and modeled values.[81,82] Finally, the newer ratios from Sheps *et al.*[78] are implemented in URMELL representing the lower limit of HCOOH production from Criegee degradation.

For the newly included oxidation product $HOCH_2OOH$, reactions with OH (R-5)[83] and photolysis ((R-6); IUPAC) are implemented. The IUPAC photolysis parameters are transformed into photolysis rate formula parameters as used in URMELL (see Tables S1-3 and S1-4†). The photolysis of $HOCH_2OOH$ produces OH and the $HOCH_2O$ radical. The reaction of $HOCH_2OOH$ with OH generates a hydroxy hydroperoxide radical $HOCH_2OO$, for which several channels are possible (R-7) till (R-10) and included in URMELL following the IUPAC recommendation. For the reaction of $HOCH_2OO$ with HO_2 (R-9) the IUPAC recommendations are uncertain as for one reaction channel two possible formulations exist. Here, we use the recommendation from Jenkin *et al.*[84] including the $HOCH_2O$ radical formation rather than the direct production of HCOOH and HO_2. For the self-reaction (R-10), only the dominant branch is considered. The most likely degradation channel for the reaction product $HOCH_2O$ is reaction with O_2 forming HCOOH with HO_2 (R-11).[83]

$$HOCH_2OOH + OH \rightarrow HOCH_2OO, \quad \text{(R-5)}$$

$$HOCH_2OOH \xrightarrow{phot} HOCH_2O + OH, \quad \text{(R-6)}$$

$$HOCH_2OO \rightarrow HCHO + HO_2, \quad \text{(R-7)}$$

$$HOCH_2OO + NO \rightarrow HOCH_2O + NO_2, \quad \text{(R-8)}$$

$$HOCH_2OO + HO_2 \rightarrow 0.5HOCH_2OOH + 0.3(HCOOH + H_2O) + 0.2(OH + HOCH_2O) + O_2, \quad \text{(R-9)}$$

$$HOCH_2OO + HOCH_2OO \rightarrow 2HOCH_2O + O_2, \quad \text{(R-10)}$$

$$HOCH_2O + O_2 \rightarrow HCOOH + HO_2. \quad \text{(R-11)}$$

2.2.2 Chemistry of the stabilized Criegee intermediate *E*-CH_3CHOO. For the stabilized Criegee intermediate *E*-CH_3CHOO, the same ratios as for the water dimer reaction of the Criegee intermediate CH_2OO are assumed (see (R-12)).

$$E\text{-}CH_3CHOO + (H_2O)_2 \rightarrow \begin{cases} 0.55 \times (CH_3CH(OH)OOH + H_2O) \\ 0.4 \times (CH_3CHO + H_2O_2 + H_2O) \\ 0.05 \times (CH_3C(O)OH + 2H_2O) \end{cases} \quad \text{(R-12)}$$

Except for the reaction rate constant of $CH_3CH(OH)OOH$ with OH (R-13), no separate data was available. Therefore, $CH_3CH(OH)OOH$ chemistry (R-14)–(R-19) was adapted analog to $HOCH_2OOH$. According to Chen *et al.*[83] and the IUPAC recommendation, the most likely degradation channel for $CH_3CH(OH)O$ is C_1–C_2 bond separation producing HCOOH and CH_3 which reacts with O_2 and produces CH_3O_2 (R-19).

$$CH_3CH(OH)OOH + OH \rightarrow CH_3CH(OH)OO, \quad \text{(R-13)}$$

$$CH_3CH(OH)OOH \xrightarrow{phot} CH_3CH(OH)O + OH, \quad \text{(R-14)}$$

$$CH_3CH(OH)OO \rightarrow CH_3CHO + HO_2, \quad \text{(R-15)}$$

$$CH_3CH(OH)OO + NO \rightarrow CH_3CH(OH)O + NO_2, \quad \text{(R-16)}$$

$$CH_3CH(OH)OO + HO_2 \rightarrow 0.5CH_3CH(OH)OOH + 0.3(CH_3C(O)OH + H_2O) + 0.2(OH + CH_3CH(OH)O) + O_2, \quad \text{(R-17)}$$

$$CH_3CH(OH)OO + CH_3CH(OH)OO \rightarrow 2HOCH_2O + O_2, \quad \text{(R-18)}$$

$$CH_3CH(OH)O \rightarrow HCOOH + CH_3. \quad \text{(R-19)}$$

2.3 Organic acyl peroxy radicals

Further updates relate to branching ratios and rate coefficients of organic acyl peroxy radicals ($RC(O)O_2$) based on recent recommendations from Jenkin *et al.*[85] Accordingly, the reaction of $CH_3C(O)O_2$ with HO_2 (R-20) was adjusted as follows (in bold new ratios in brackets old ratios):

$$CH_3C(O)O_2 + HO_2 \rightarrow \begin{cases} \mathbf{0.37}(0.4) \times (CH_3C(O)OOH + O_2) \\ \mathbf{0.13}(0.2) \times (CH_3COOH + O_3) \\ \mathbf{0.5}(0.4) \times (CH_3C(O)O + OH + O_2) \end{cases} \quad \text{(R-20)}$$

The reaction product $CH_3C(O)O$ decomposes into CO_2 and CH_3 and subsequent O_2 reaction produces CH_3O_2. Furthermore,

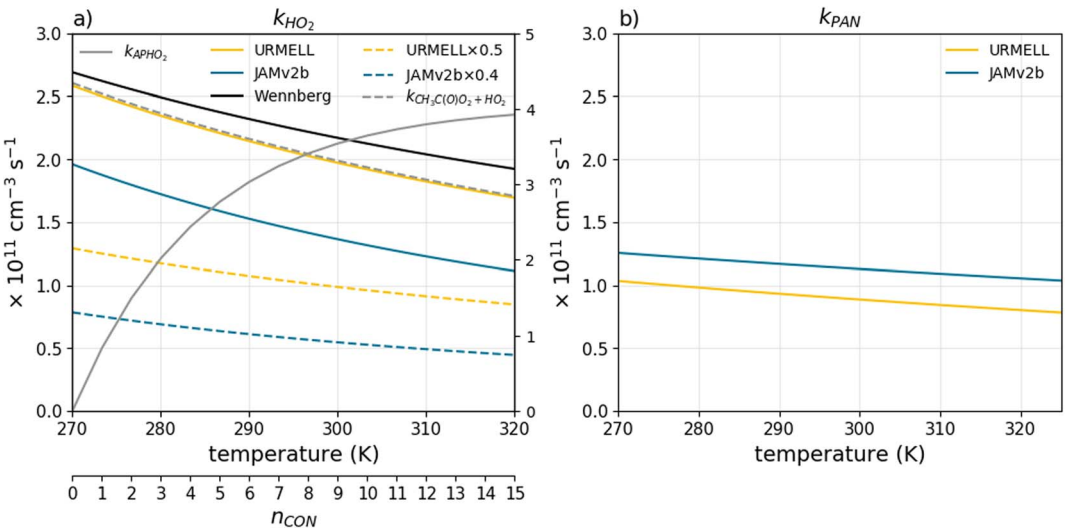

Fig. 1 Temperature dependent reaction rate coefficient for (a) the reaction of $CH_3C(O)O_2$ with HO_2 k_{HO_2}, as well as the product of k_{HO_2} and the ratio for the third channel producing OH and CH_3O_2 together with k_{APHO_2} as a function of n_{CON} and k_{APHO_2} for $CH_3C(O)O_2$; (b) the reaction of $CH_3C(O)O_2$ with NO_2 k_{NO_2} leading to PAN. Moreover, the branching ratios for the reactions of $RC(O)O_2$ with CH_3O_2 (R-21) and $CH_3C(O)O_2$ (R-22) are adapted based on the IUPAC recommendations for $CH_3C(O)O_2$.

the reaction rate constant changed from $5.2 \times 10^{-13} \times \exp(980/T)$ (MCM3.3.1) to $1.73 \times 10^{-12} \times \exp(730/T)$. This results in a faster reaction and a higher OH and CH_3O_2 production (see Fig. 1a). Note Wennberg *et al.*[30] uses the previous IUPAC recommendation before the latest change in preferred values in 2019 occurred resulting in slightly higher k_{HO_2} values than the actual one (see black line in Fig. 1a). The recommendations of Jenkin *et al.*[85] have further been applied to $CH_3C(O)O_2$-radical equivalent reactions of $RC(O)O_2$ with HO_2 using the Jenkin *et al.*[85] formula k_{APHO_2}. k_{APHO_2} is visualized in Fig. 1a for 298 K as a function of carbon, nitrogen and oxygen atom number n_{CON} (excluding the peroxy radical oxygen atoms) in gray. With increasing atom number the HO_2 reaction rate coefficient increases. For $n_{CON} = 3$ excellent agreement with the IUPAC recommendation for $CH_3C(O)O_2$ is reached (gray dashed line in Fig. 1a).

$$RC(O)O_2 + CH_3O_2 \rightarrow O_2 + 0.9CH_3O + 0.9RC(O)O + 0.1RC(O)OH + 0.1HCHO \quad (R\text{-}21)$$

$$RC(O)O_2 + CH_3C(O)O_2 \rightarrow RC(O)O + CH_3C(O)O + O_2 \quad (R\text{-}22)$$

CH_3O forms HCHO and HO_2 after oxidation by O_2 (MCM3.3.1). The reaction rate constants of $RC(O)O_2$ with CH_3O_2, $CH_3C(O)O_2$, NO, NO_3 and NO_2 are also based on IUPAC preferred values for $CH_3C(O)O_2$ if not stated otherwise in Table S1-2.†

The reaction of $RC(O)O_2$ radicals with NO_2 leads to the formation of PANs. Changes to the reaction rate constant describing PAN formation or decomposition can impact the NO_x as well as the O_3 budget, as they are closely linked. In URMELL, PAN formation and decomposition follow the IUPAC recommendations, but the rate coefficient for PAN formation $k_{troe}(3.28 \times 10^{-28}, -6.87, 0, 1.125 \times 10^{-11}, -1.105, 0, 0.3)$ differs from the one applied in JAMv2b $k_{troe}(2.7 \times 10^{-28}, -7.1, 0, 1.2 \times 10^{-11}, -0.9, 0, 0.6)$. For calculation specifications see ESI S1.† Both functions are shown in Fig. 1b for 1 atm (molecular density $M = 7.34 \times 10^{21}/T(K)$) and varying temperature values. A sensitivity study was carried out to investigate the impact of the updated reaction rate constant. An additional sensitivity study was performed addressing the overall change on $RC(O)O_2$ chemistry. For the sake of clarity, the results are discussed in more detail in the ESI S2.2.1.† Both sensitivity studies indicate an increase in O_3, OH, HO_2, NO, NO_2, NO_3 and HNO_3 peak concentrations for the updated $RC(O)O_2$ reaction pathways.

2.4 Advanced oxidation scheme for aromatic compounds

As outlined before, the present study aims at an improved air quality modeling in urban environments, thus the treatment of anthropogenic SOA sources, *e.g.* from aromatic compounds was revised and extended. The original JAMv2b mechanism describes the oxidation of benzene, toluene and lumped xylenes as well as their corresponding phenols (PHENOL, CRESOL, XYLOL). The oxidation with OH of these monohydroxy phenols form ring-opening products (peroxyl radicals; $BENZO_2$, $TOLO_2$, $XYLO_2$), lumped aromatic 1,2-diols (CATECHOL) and lumped phenoxy radicals (C_6H_5O). The latter are currently implemented to yield nitrophenols when reacting with NO_2. Nitrophenols are not very reactive towards OH radicals and are thus determined as sticky nitrate compounds.[39] Therefore, in the previous studies using JAMv2b, their fate was determined by deposition rather than oxidation processes. However, aromatic compounds with an added hydroxyl group are sensitive towards oxidation by NO_3 radicals (IUPAC, MCM3.3.1). Therefore, oxidation by NO_3 radicals might determine their oxidative fate in urban polluted environments, where the conditions of high NO_x and ozone concentrations enable stronger NO_3-radical formation. As the mechanism URMELL is projected to be applied for such environments, the formation of nitro-hydroxy compounds and its further oxidation by OH and NO_3 radicals have been included. The same applies for the formation of aromatic nitro-dihydroxy compounds, reaction products of CATECHOL. The further oxidation of these nitro-hydroxy and -dihydroxy products leads to highly oxidized molecules with extremely low vapor pressures.

Furthermore, the oxidation of monohydroxy phenols with NO_3 form lumped phenoxy radicals (C_6H_5O), ring-opening products without ($PHENO_2$, $CRESO_2$) and with an ON(=O)=O group ($NPHENOLO_2$, $NCRESO_2$). The formation of the latter products is handled very differently between different mechanisms and are in general not treated explicitly in reduced mechanisms.[37,39,43,86] A sensitivity study, considering three different approaches for the handling of the phenol + NO_3 reaction channels can be found in the ESI Sect. S2.2.† In JAMv2b $NPHENOLO_2$ and $NCRESO_2$ are approximated with $PHENO_2$. While this has no significant impact for warmer temperatures and longer solar radiation periods (see Sec. 4.1 summer cases) it gains in importance for colder temperatures and longer nights. Then significant amounts of NO_3 can form which facilitate NO_3 degradation channels. When including $NPHENOLO_2$ and $NCRESO_2$ their further oxidation by NO, NO_3, CH_3O_2 and $CH_3C(O)O_2$ produces NO_2 while when using $PHENO_2$ HO_2 is released. This has major impacts on the entire oxidizing capacity especially when reducing the solar radiation impacts (see Sect. 4.3 and ESI S2† winter_05 case). The oxidation of $NPHENOLO_2$ and $NCRESO_2$ with HO_2 leads to NPHENOLOOH and NCRESOOH, two additional SOA precursor substances. Further possible SOA branches are included by integrating nitrate formation (BENZN, TOLN, XYLN) from bicyclic peroxy radical ($BENZO_2$, $TOLO_2$, $XYLO_2$) reactions with NO and their OH reaction products (BENZ=O, TOL=O).

Additionally, the reaction pathways of aromatic RO_2 radicals are extended by using the product yields given in MCM3.3.1. So far, only the reaction products glyoxal, methylglyoxal and the lumped species for unsaturated oxidized aldehydes (BIGALD1, BIGALD2, BIGALD3, BIGALD4) are considered in JAMv2b. For the unsaturated oxidized aldehydes, only photolysis processes are considered in JAMv2b. In URMELL, also reactions with OH, NO_3 and ozone are added following MCM3.3.1. Other products of aromatic RO_2 radicals such as unsaturated organic acids, furanones, quinones and anhydrides as described in the MCM3.3.1 are missing in JAMv2b. As a consequence, the carbon balance is not closed and possible important SOA pathways are neglected. To overcome this gap, these potential SOA precursor

species are incorporated into URMELL. The unsaturated oxidized organic mono acids are represented by the lumped species BIGACID1, BIGACID2 and BIGACID3 in accordance to BIGALD compounds for unsaturated oxidized aldehydes. Furanones, quinones as well as anhydrides are represented by the lumped species BZFUONE, FUONE, BZQONE and MALANHY, respectively (Table S1-1†). Also, the photolysis products of BEPOMUC and TEPOMUC are adjusted to include the SOA products C5DIALOOH and C615CO2OOH.

2.5 Advanced isoprene chemistry implementation

In addition to aromatics, the chemistry of isoprene is extended to incorporate the latest state-of-the-art knowledge, including subsequent reaction pathways of formed products such as methyl vinyl ketone (MVK) and methacrolein (MACR). These follow, *e.g.* the comprehensive study of Wennberg *et al.*[30] but with a few adaptations. In the following, a brief description of these adaptations is presented, including changes to the isoprene NO_3 and OH chemistry within the next two subsections. For isoprene + O_3, only the treatment of the stable Criegee intermediate CH_2OO changed as outlined in Sect. 2.2.1. For initial isoprene reactions with NO_3, OH and ozone, the latest IUPAC task group reaction rate constant recommendations are used (Table S1-2†).

Specific isoprene oxidation products are lumped to reduce the complexity of URMELL where feasible. The lumped products are labelled with an L as first letter of their lumped group name. Here, the reaction rate constant is a weighted constant based on the contribution to the lumping group and the individual rate constant of the single compound. The overall reaction product ratios are also calculated using the contribution of the single reaction pathways to the lumping group. Reactions of radicals with O_2 are assumed to occur instantaneously, therefore these intermediate steps are skipped following the MCM3.3.1 implementation.

2.5.1 Isoprene + NO_3. According to Wennberg *et al.*,[30] the NO_3-initiated isoprene oxidation produces peroxy radicals with a nitrate group (INO_2) which are lumped into two species: 46.5% NISOPBO$_2$ (90% β-1,2-INO_2; 10% β-4,3-INO_2) and 53.5% NISOPDO$_2$ (84% σ-1,4-INO_2; 16% σ-4,1-INO_2). The further degradation of NISOPDO$_2$ generates HO_2, NO_2, an C_5 aldehyde (NC4CHO) and an organic radical (NISOPO), while the further oxidation of NISOPBO$_2$ yields HCHO, NO_2, MVK and MACR. But, the proposed decomposition of NISOPBO$_2$ can induce high night-time production rates of MVK. To scrutinize the impact of this channel, initial box model simulations were performed including the recommended degradation in URMELL. The simulations showed three times higher MVK concentrations under high NO_x conditions. A study by Vereecken *et al.*[87] reported an overestimation of both MVK and MACR between 250 to 400%. They attribute this to the complete conversion of β-1,2-INO_2 to MVK, whereas their study favors the formation of peroxy radicals with a nitrate and epoxide group (NISOPEOO1). For the implementation of this scheme, the ratio between the *anti*- (68%; NISOPEOO1E) and *syn*-1-NO_3-2,3-epoxy-isoprene-4-OO (32%; NISOPEOO1Z) was determined for 298 K using the pseudo-steady-state approximation[88] for the ring opening/closing and oxidation by O_2. This is in agreement with the results of Vereecken *et al.*[87] (68 ± 2% NISOPEOO1E).

Within the NISOPBO$_2$ scheme, the contribution from β-4,3-INO_2 plays only a minor role. Therefore, only β-1,2-INO_2 is considered for NISOPBO$_2$ chemistry in URMELL including the formation of NISOPEOO1 isomer following Vereecken *et al.*[87] The majority of oxidation steps of NISOPEOO1E produce MACRN + HCHO + HO_2 and a product with a carbonyl, nitrate and epoxide group (ICNE) + HO_2. In the temperature interval of 270 to 315 K, the yields for the MACRN and ICNE pathways range from 63–87% and 37–13%, respectively. For URMELL, fixed ratios for 298 K are implemented yielding 80% MACRN and 20% ICNE. For ICNE, the OH-pathway described by Wennberg *et al.*[30] leading to OH + 2CO + 0.35NOA + 0.65MGLY + 0.65NO_2 + 0.65HO_2 is assumed to occur immediately. As this reaction directly regenerates OH, this has no effect on the OH budget. The NISOPEOO1Z pathways mainly leads to LIECHO + NO_2 formation.

2.5.2 Isoprene + OH. The OH oxidation is the major loss process for isoprene resulting into a highly complex system of different isomers.[30,89] OH-addition to the C=C double bonds of isoprene is possible at four positions: C1, C2, C3 and C4, whereby terminal OH-addition dominates. Thus, only the terminal products are considered (63% C1 and 37% C4) in URMELL. The remaining second double bond can take two alignments creating *cis*/*trans* alkyl radicals which undergo a reversible O_2-addition creating a pool of various isoprene peroxy radicals (ISOPOO). The peroxy group of the ISOPOO-isomer is either in β- or δ-position. As the degradation pathways between the ISOPOO-isomers differ substantially, it is crucial to capture the ISOPOO-composition adequately. Teng *et al.*[89] investigated this system and determined, that roughly 95% of ISOPOO is of β O_2-addition under most atmospheric relevant conditions. This is much higher compared to the kinetic distribution and the reason for the shift in ISOPOO distribution between JAMv2b and URMELL. In JAMv2b, the reaction of isoprene and OH yields:

$$C_5H_8 + OH \rightarrow 0.4\text{LISOPACO}_2 + 0.35\text{ISOPBO}_2 + 0.25\text{ISOPDO}_2, \quad \text{(R-23)}$$

and in URMELL:

$$C_5H_8 + OH \rightarrow 0.05\text{LISOPACO}_2 + 0.6\text{ISOPBO}_2 + 0.35\text{ISOPDO}_2. \quad \text{(R-24)}$$

The new branching is in agreement with Wennberg *et al.*[30] and Müller *et al.*[76] The contribution of δ O_2-addition to the 1-OH system is about 5% and for the 4-OH system 6%.[64] Within MAGRITTE[76] and the reduced mechanisms of Wennberg *et al.*,[30] the β- and δ-isomers are lumped within their OH system resulting in two ISOPOO reaction products. In URMELL, β-isomers are treated separately: ISOPBO$_2$ for the 1-OH and ISOPDO$_2$ for the 4-OH system. While the δ-isomers are grouped into LISOPACO$_2$ with a ratio of 60 : 40 for the 1-OH:4-OH system,

respectively. For β-isomers, the 1,5 H-shift and for *cis*-δ-isomers the 1,6 H-shift is implemented following Wennberg *et al.*[30] These H-shift reactions are a major HO_x recycling pathways and can significantly impact OH, HO_2, ozone and NO_3 concentrations. This is further analyzed by a sensitivity study and discussed in the ESI S2.2.4.† Most parts of the OH-driven isoprene chemistry follow the full mechanism of Wennberg *et al.*[30] Unfortunately, for some reaction products no subsequent reactions are listed, such as ISOP1OH4OH, ISOP1OH2OH and ISOP3OH4OH. Here, the reactions for ISOPAOH, ISOPBOH and ISOPDOH of the MCM3.3.1 are implemented in URMELL. To reduce the complexity of the system, also the recommendations for the reduced mechanism of Wennberg *et al.*[30] are considered such as for aldehyde peroxyl radicals with (i) two hydroperoxyl or (ii) a hydroperoxyl and a hydroxyl group. Here, only H-shifts are considered as they are assumed to outcompete all bimolecular chemistry.[30]

2.6 URMELL compared to other mechanisms

In summary, the developed mechanism URMELL contains 313 species and 916 reactions. Compared to other reduced mechanisms this is much more sophisticated as for example RACM with around 100 species and 300 reactions, or JAMv2b with around 200 species and a bit more than 500 reactions. However, URMELL is still more condensed than the nearly explicit MCM3.3.1 with more than 5500 species and around 14 000 reactions, and applicable for 3D CTMs. While for aromatics most updates follow the MCM3.3.1, additional adjustments are performed based on recent findings which have not been included into a CTM chemical mechanism to this extent before or the MCM3.3.1. This already starts at the fundamental basics, the HO_x, NO_x and O_x systems itself, followed by changed chemical treatments of $RC(O)O_2$ as well as ozonolysis reactions including stabilized Criegee intermediates and goes beyond isoprene. Although, newer mechanism focusing on isoprene exists, they were released before new findings on isoprene–NO_3-chemistry became available.[76,90] In the next sections, the impact of these changes on the tropospheric gas-phase composition are emphasized through both box model and CTM simulations.

3 Design of model simulations

To evaluate the impact of all changes previously stated, the performance of URMELL is analyzed using box model simulations for several environmental scenarios and is compared with other chemical mechanisms of varying complexity (RACM, JAMv2b, MCM3.3.1). For this first task, the box model SPACCIM, the Spectral Cloud Chemistry Interaction Model is used (Sect. 3.1).[91] Secondly, URMELL is applied in the chemical transport model COSMO-MUSCAT[64,92] and examined through comparisons with multiple measurement sites for ozone, NO and NO_2 (Sect. 3.2). For the evaluation, time series analyses are frequently used. To gain knowledge about the linear relationship between modeled and/or measured data, Pearson correlation values are calculated with Python. But, even though time series show a good agreement between their curve progression, they still may differ significantly in absolute values. Therefore, the coefficient of divergence (COD) is given in addition and calculated as follows:

$$\mathrm{COD} = \sqrt{\frac{1}{n}\sum_{i=1}^{n}\left(\frac{x_i - y_i}{x_i + y_i}\right)^2}$$

where n is the number of data points, x_i is the concentration of one of the mechanisms to be compared with y_i the reference data set concentration at time step i.[93] The COD is a measure of variability and can reach values close to 1 for low similarity and values close to zero for high similarity or even equal zero if identical concentrations are present between the compared datasets. This is applied to box model simulations in Sect. 4 comparing the comprehensive MCM3.3.1 with the reduced mechanisms (RACM, JAMv2b, URMELL), as well as CTM simulations in Sect. 5.

3.1 Box model simulation with SPACCIM

For the mechanism comparison using the box model SPACCIM, the near explicit Master Chemical Mechanisms version 3.3.1 (MCM3.3.1) is used and functions as the benchmark mechanism throughout the box model analysis. Additionally, JAMv2.b, which was the starting point of URMELL, and an extension of the Regional Atmospheric Chemistry Mechanism RACM-MIM2-ext[4,37,63] hereafter called RACM are considered. RACM has been extensively used for air quality studies within the chemical transport model COSMO-MUSCAT and is used as reference simulation for the 3D chemistry transport model simulations of Sect. 5.[4,65,94,95] For all box model simulations, the MCM3.3.1 is considered as the reference point, as this is currently the most sophisticated mechanism available.[96] Therefore, given correlation and COD values hereafter always refer to the MCM3.3.1, if not stated otherwise.

The box model simulations are carried out for 45°N to define the period of solar radiation and zenith angle. Two different emission scenarios are considered: remote and urban which have been previously used with SPACCIM.[99–103] The emission values are based on Guenther *et al.*,[97] and EDGAR v2,[98] respectively. But as RACM contains lumped species, the emissions are split into the individual species of the different chemical mechanisms (MCM, JAMv2b, URMELL) by using the fractions provided by Middleton *et al.*[104]

The urban case comprises higher anthropogenic emissions, *e.g.* for NO_x and aromatics, while the remote case comprises lower NO_x and higher BVOC emissions. The emissions are implemented as constant fluxes throughout the entire simulation period. Note, that this causes deviations from real emissions of anthropogenic as well as natural origins. However, this emission set-up is used for all mechanisms giving a systematic error and thus, for mechanism comparisons this approach is feasible.

To also account for deviating conditions, a summer (indicated by _s) and a winter (indicated by _w) case are simulated, which are initialized for the 19th of June and 19th of December

Table 1 Overview of performed box model simulations with SPACCIM

	Emission		Season		Photolysis rate	
Scenarios	Urban	Remote	Summer	Winter	Full	Halved
urb_s_1	x		x		x	
urb_s_05	x		x			x
urb_w_1	x			x	x	
urb_w_05	x			x		x
rem_s_1		x	x		x	
rem _s_05		x	x			x
rem _w_1		x		x	x	
rem _w_05		x		x		x

with a constant boundary layer temperature of 280 K and 273 K, respectively. Additionally, different radiation conditions are investigated by either no attenuation of incoming radiation (indicated by _1), or an attenuation of incoming radiation by 50% (indicated by _05) resulting in halved photolysis rates. An overview about all scenarios is given in Table 1. The first 24 h are used as spin-up time. Therefore, the plots (Fig. 1, 2 and S2-1 till S2-6†) always start at 24 h and run until 96 h (showing 20.06. −22.06 or 20.12. −22.12.) and also the performed statistics (Tables 3, 4 and S2-1†) include these three model days, only.

Please note that the present study is a theoretical study to analyze the performance of the different mechanisms between each other under various environmental conditions. Thus, the results from the box model cannot directly be transferred to the

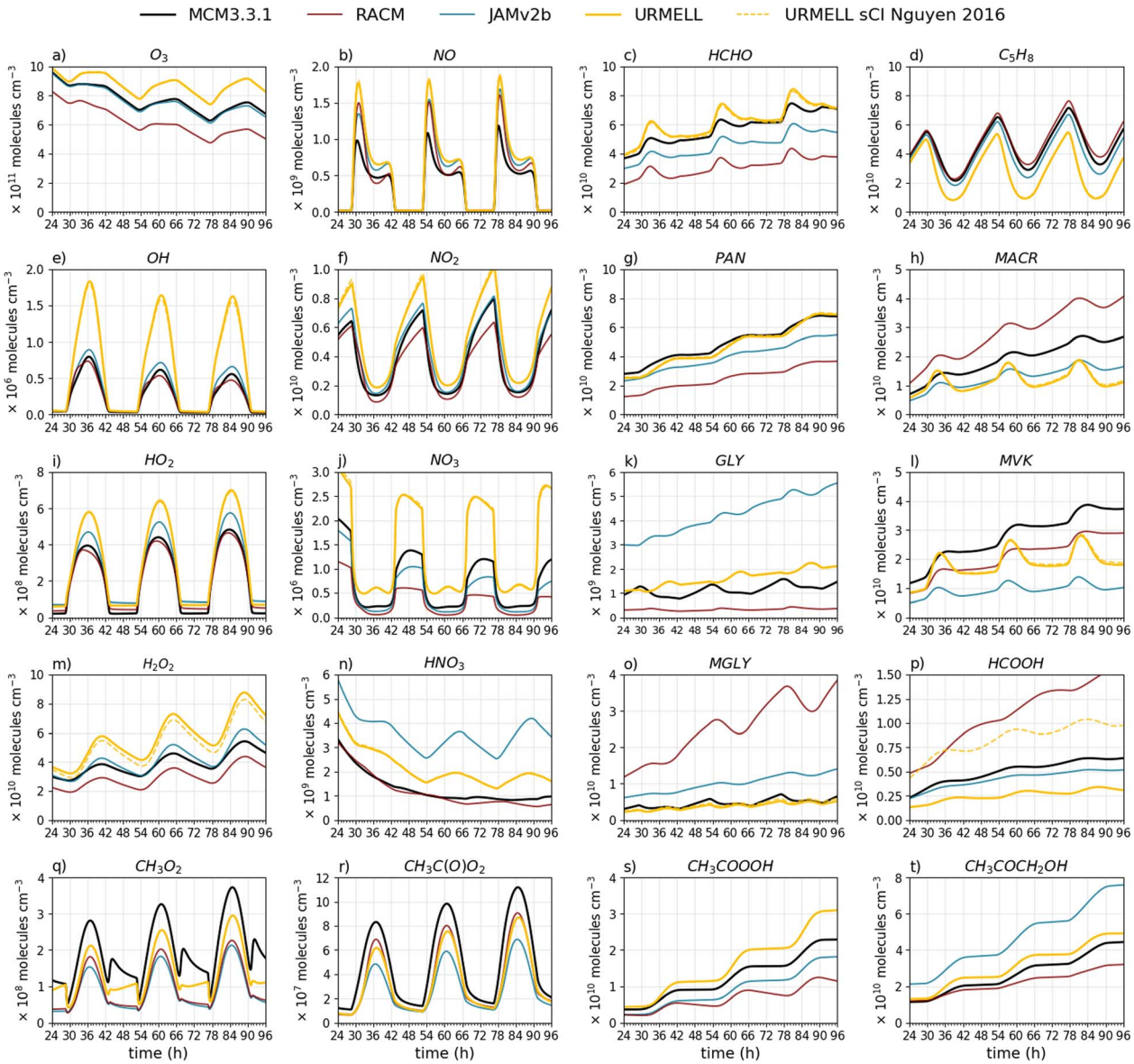

Fig. 2 Time series of (a) O_3, (b) NO, (c) HCHO, (d) C_5H_8, (e) OH, (f) NO_2, (g) PAN, (h) MACR, (i) HO_2, (j) NO_3, (k) GLY, (l) MVK, (m) H_2O_2, (n) HNO_3, (o) MGLY, (p) HCOOH, (q) CH_3O_2, (r) $CH_3(O)O_2$, (s) CH_3COOOH and (t) CH_3COCH_2OH for the remote summer case with clear sky conditions modeled with MCM3.3.1 (black line), RACM (red line), JAMv2b (blue line) and URMELL (yellow line) as well as a sensitivity run including the branching ratios of Nguyen *et al.*[79] for the Criegee intermediate CH_2OO (yellow dashed line).

reality and should be seen as extreme events to test the sensitivity of the mechanisms. But the studies can still provide insights on the concentration magnitude and help to identify important night- and day-time path ways and eventually on temporal profiles. For the mechanism comparison, 20 chemical compounds are considered. To investigate the effects of the updates to isoprene chemistry, isoprene and its reaction products MACR and MVK as well as the multi-generation product CH_3COCH_2OH are chosen. Additional common reaction products from various sources considered for the comparison are HCOOH, MGLY, GLY, HCHO, CH_3COOOH, CH_3O_2 and CH_3CO_3. Other substances of interest are O_3 and OH, HO_2, H_2O_2, HNO_3, NO, NO_2, NO_3 and PAN. All chemical compounds chosen are treated explicitly in the different mechanisms (no lumped compounds) except in RACM where MACR, PAN, CH_3COOOH (PAA), CH_3COCH_2OH (HKET) and MGLY are lumped species.

3.2 CTM simulations with COSMO-MUSCAT

The comparison through box model comparisons has limitations with regard to advection, entrainment and deposition. In order to evaluate and verify the quality of URMELL for air quality modeling, it has been applied in the CTM COSMO-MUSCAT.[64] Simulation results are compared with a simulation using the COSMO-MUSCAT default gas-phase mechanism RACM. The model system COSMO-MUSCAT and its good performance has been confirmed through multiple model intercomparison studies.[105–108]

The period May 2014 is chosen for the model domain of Germany, as for this episode a detailed sensitivity study was carried out recently by Luttkus *et al.*[4] The simulations are initialized for the 20th of April 2014. The time period until the 1st of May is used as spin-up while the entire May is used for the CTM simulation analysis. Additionally, a time period in spring enables a closer look at the model performance under varying meteorological conditions. At the 19th of May, a frontal system passes the model domain accompanied by rain and the formation of a high-pressure system afterwards. On the 20th of May calm winds, high solar radiation and warm temperatures boost BVOC emissions while at the same time their distribution is limited facilitating local degradation processes after a washout event. Therefore, the 20th of May is selected for further analysis. For both COSMO-MUSCAT simulations, the detailed land use data set with 138 land use categories is used together with the agricultural biomass density enhancement (for more detail about the model system and setup, the reader is referred to Luttkus *et al.*[4] and references within). However, a few modifications have been made within the model setup compared to Luttkus *et al.*,[4] which are outlined hereafter. Firstly, the outer European model domain providing the initial and boundary conditions for the inner German domain is enhanced and has a finer resolution of 14 km × 14 km now. Secondly, the deposition flux calculation changed from a bulk to a mosaic approach. Meaning, that instead of dominant or weighted average values for every grid cell, individual contributions of all appearing land use categories within a grid cell are considered, now. Both of these changes apply for RACM and URMELL simulations.

Additionally, URMELL considers more BVOCs as RACM and thus, for simulations with URMELL, the BVOC emission and deposition module are adapted as follows. The BVOC emission model distinguishes between 17 monoterpenes,[109] while URMELL considers only four monoterpene clusters: α-pinene, β-pinene, myrcene and limonene. Therefore, all cyclic monoterpenes with a terminal C=C double bond (β-pinene, camphene, sabinene) are lumped into β-pinene (BPIN) and with an inner C=C double bond (α-pinene, Δ^3-carene, α-thujene) into α-pinene (APIN). Cyclic monoterpenes with multiple C=C double bonds (limonene, α- and γ-terpinene, α- and β-phellandrene) are grouped into limonene (LIMONENE) and acyclic monoterpenes (myrcene, *trans*- and *cis*-ocimene, linalool) into myrcene (MYRC). *P*-cymene is an aromatic compound and treated as xylene (XYL). 1,8-cineol is a bicyclic ether and a monoterpenoid from limonene, thus it is treated as the monoterpene reaction product TERPROD1, that represents all C10 secondary products of terpene oxidation. An overview of the monoterpene assignment is given in Table 2. Unlike RACM, the smaller BVOCs methanol, acetone, ethanol, acetaldehyde, formaldehyde, formic acid, and acetic acid are treated individually in URMELL. Therefore, the BVOC emission algorithm was adapted accordingly.

The dry deposition scheme implemented in COSMO-MUSCAT is based on Schlünzen *et al.*[110–112] and essentially considers all RACM species. In each case, the dry deposition flux is the product of the species concentration and the deposition velocity, which is calculated based on a resistance model and is the reciprocal value of the aerodynamic, the sublayer and the surface resistance. Overall, the deposition depends on the atmospheric stability, land use type, season, solar irradiation, relative humidity and gaseous species (solubility, reactivity). The scheme used was adapted and extended to URMELL species based on functional group composition (see Table S1-1†). But unfortunately, information of the deposition velocity or resistances for multifunctional

Table 2 Assignment of the emitted 17 monoterpenes to the corresponding URMELL species

URMELL species	APIN	BPIN	MYRC	LIMONENE	XYL	TERPROD1
Emitted monoterpenes	α-Pinene, Δ^3-carene, α-thujene	β-Pinene, camphen, sabinene	Myrcene, *trans*-ocimene, *cis*-ocimene, linalool	Limonene, α-terpinene, γ-terpinene, α-phellandrene, β-phellandrene	*p*-Cymene	1,8-Cineol

molecules are scarce. Therefore, measurements from Nguyen *et al.*[113] for a temperate forest were used as a guideline. While for hydroperoxides with an additional hydroxyl or carbonyl group the surface resistance is small (as for methyl hydrogen peroxide (OP) and peroxyacetic acid (PAA), respectively), it gets higher for compounds with at least one carbonyl and hydroxyl and/or nitrooxy group (similar to formic acid (ORA)). All peroxy radicals are set to peroxides (RO_2), all peroxyacetyl nitrates to PAN and substances with one or more carbonyl groups to acetaldehyde (MeCHO). Even though, more sophisticated deposition schemes are available,[114–116] the implementation of a new deposition scheme into COSMO-MUSCAT is beyond the scope of this paper, but will be the subject of future model development.

In the following section, results from box model and CTM simulations are presented and discussed.

4 Box model results

To test the updates presented in the previous section multiple box model simulations are performed with SPACCIM for two emission scenarios (remote and urban) and various meteorological condition. Especially for the remote case URMELL predicts much higher peak oxidant concentrations *e.g.* O_3, OH and NO_3 radicals. To further quantify the sources leading to these increased oxidant concentrations, multiple sensitivity studies are performed for the rem_s_1 scenario and analyzed. The main results are presented hereafter and a more detailed analysis can be found in the ESI S2.3.†

4.1 Sensitivity study for the remote case

In contrast to the updates on aromatic chemistry, most modifications in isoprene chemistry implemented in URMELL are not part of the current MCM3.3.1. Therefore, deviations within

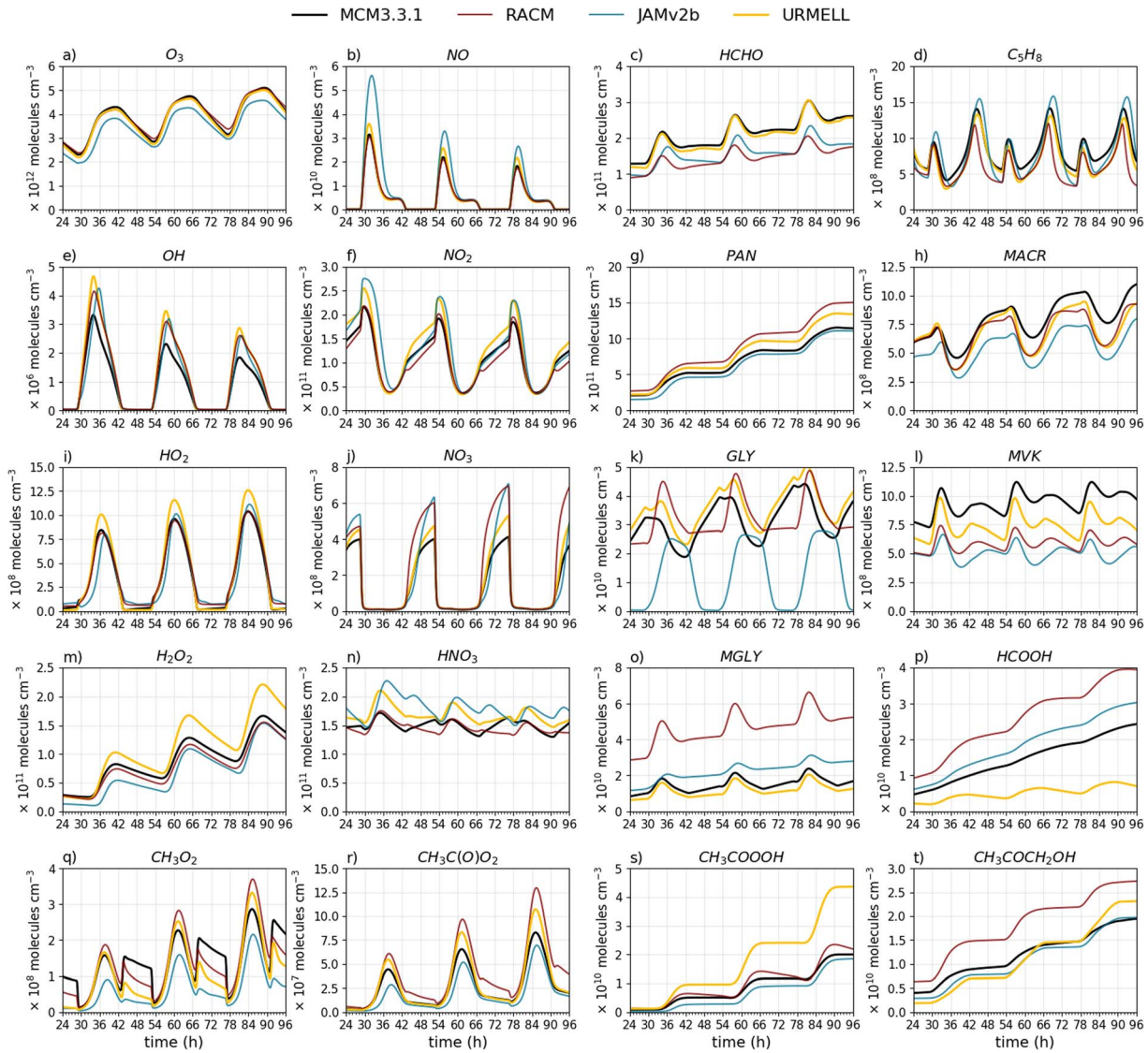

Fig. 3 Time series of (a) O_3, (b) NO, (c) HCHO, (d) C_5H_8, (e) OH, (f) NO_2, (g) PAN, (h) MACR, (i) HO_2, (j) NO_3, (k) GLY, (l) MVK, (m) H_2O_2, (n) HNO_3, (o) MGLY, (p) HCOOH, (q) CH_3O_2, (r) $CH_3(O)O_2$, (s) CH_3COOOH and (t) CH_3COCH_2OH for the urban summer case with clear sky conditions modeled with MCM3.3.1 (black line), RACM (red line), JAMv2b (blue line) and URMELL (yellow line).

Table 3 Overview of the different sensitivity studies and their considered modifications

Sensitivity study	PAN	$RC(O)O_2$	Phot.	GLY	O_3	MVK & MACR	C_5H_8	H-shift
1: PAN	x							
2: $RC(O)O_2$	x	x						
3: Photolysis	x	x	x					
4: GLY & O_3	x	x	x	x	x			
5: C_5H_8	x	x	x	x	x	x	x	x

the remote scenario simulations will occur more likely (Fig. 2). For the OH radical, the modeled concentration peak is a factor of two to three higher. The modeled OH concentration levels of URMELL reach up to 1.75×10^6 molecules per cm^3 for clear sky conditions (Fig. 2e) while the other mechanisms do not reach 10^6 molecules per cm^3, which is in contrast to the urban case, where all mechanisms simulated noon values above 10^6 molecules per cm^3 (Fig. 3e). But, measurements from isoprene-dominated regions would support higher OH values as modeled by URMELL.[10,117–120]

For the rem_1_s sensitivity studies, the reactions of the updated reaction scheme (described in Sect. 2) are stepwise reset to JAMv2b reaction equations. At first, non-isoprene related updates are analyzed starting with the changed $RC(O)O_2$ chemistry which comprises two simulations: (i) solely changed k_{NO_2} rate coefficient and (ii) total $RC(O)O_2$ related updates (Sect. 2.3). All reactions considered for these two studies are indicated by 1 and 2 in Table S1-2.† In a next step, the impact of changed photolysis rates and products are analyzed (Sect. 2.1, Table S1-3† indicated by 3). Finally, the change in GLY rate constant (Sect. 2.1) and ozonolysis implementations (Sect. 2.2) are investigated (Table S1-2† indicated by 4). Afterwards, the isoprene related effects including initial oxidation steps, H-shift reactions as well as MVK and MACR updates are examined (Sect. 2.5, indicated by 5 in Table S1-2†). Note, that due to the stepwise resetting to JAMv2b scenario 5 includes all changes indicated by step 1 through 5, for scenario 4 it is 1 through 4 and so on. For the original JAMv2b equations the reader is referred to the corresponding publication.[39] Table 3 summarizes the presented sensitivity studies of Fig. S2-1† and the considered adjustments.

In the following, the main results are summarized, but a more detailed analysis is given in the ESI S2.3.† Roughly half the difference of O_3 (Fig. S2-1a†) and OH (Fig. S2-1e†) increase is caused by non-isoprene related changes mainly $RC(O)O_2$ chemistry (Sect. S2.3.1†) and photolysis processes (Sect. S2.3.2†). The other half is due to isoprene chemistry primarily by the newly implemented H-shift reactions of ISOPOO and the ISOPOO pool distribution itself (Sect. 2.5.2 and S2.3.4†). The ISOPOO pool composition impacts O_3 through LHC4ACCHO, MVK and MACR ozonolysis and indirectly through formation and degradation pathways of the isoprene nitrates $LISOPACNO_3$, $ISOPBNO_3$ and $ISOPDNO_3$. NO_3 (Fig. S2-1j†) reduces throughout all changes but most significantly for isoprene chemistry updates which is primarily caused by MPAN chemistry as well as lower NO_2 (Fig. S2-1f†) and O_3 (Fig. S2-1a†) concentrations mitigating the major NO_3 production pathway (Sect. S2.3.4†). The increase in day-time NO_3 is caused by the oxidation of MPAN (reaction product from MACR) by OH or O_3. Additionally, the changed $RC(O)O_2$ k_{NO_2} rate constant also notably impacts NO_3 concentrations (Sect. S2.3.1†).

Photolysis processes impact the HO_y budget (Fig. S2-1e, i and m†) as well as HCHO, CH_3O_2, $CH_3C(O)O_2$, GLY (Fig. S2-1k†) and MGLY (Fig. S2-1o†) concentrations (Sect. S2.3.2†). Compared to JAMv2b, the most significant effects on GLY is from the changed NO_3 reaction rate constant (Sect. S2.3.3†). But in comparison to MCM3.3.1 changes to isoprene chemistry (internal OH addition channels) are the driving factors (Sect. S2.3.4†). A substantial increase in HCOOH (Fig. S2-1p†) is evoked by high JAMv2b yields from MVK ozonolysis (Sect. S2.3.4†). $CH_3C(O)O_2$ (Fig. S2-1r†) is governed by changes to its rate constants (Sect. S2.3.1†) and photolysis reactions (Sect. S2.3.2†). $CH_3C(O)O_2$ reaction product CH_3COOOH (Fig. S2-1s†) is coupled to HO_2 rate coefficient and $CH_3C(O)O_2$ concentration changes. Furthermore, $CH_3C(O)O_2$ chemistry governs day-time while ozonolysis processes dominate night-time CH_3O_2 production (Fig S2-1q†). In JAMv2b ozonolysis processes have no significant impact on CH_3O_2 concentrations. In URMELL a much higher CH_3O_2 yield of 0.407 for C_5H_8 ozonolysis is implemented and due to its fast reaction rate coefficient a continues rise until 5 a.m. is observed. But due to missing ozonolysis CH_3O_2 sources such as from BIGENE, CH_3O_2 is still lower than the MCM3.3.1 (this is addressed further in Sect. 4.3). On the other hand MCM3.3.1 may provide overestimated CH_3O_2 ozonolysis yields based on recommendations from Cox *et al.*[73] Furthermore, BIGENE often have slower O_3 reaction rate coefficients which makes them less efficient with decreasing O_3 concentrations and therefore result in opposing night-time trends.

Please note, that especially all the non- but also the isoprene related modifications effect not only the remote but also dominate the alterations in the urban cases for which no separate sensitivity study is presented.

4.2 Remote case

URMELL predicts much higher oxidant concentration (Fig. 2 and S2-5–S2-7†) linked to isoprene (*e.g.* OH recycling, ISOPOO pool) and non-isoprene related changes (*e.g.* $RC(O)O_2$, photolysis) as described before. For all remote cases, correlation coefficients (see Table 4 and S2-1†) of O_3, OH, NO, NO_2, NO_3 and HO_2 are high for all mechanisms ($R > 0.9$). One exception is O_3 for URMELL ($R = 0.881$), for which a slightly increasing trend is modeled in the end in comparison to the slightly decreasing trend of the MCM3.3.1 (Fig. 2a). In the case of reduced actinic radiation (Fig. S2-5†), the difference between peak O_3, OH, NO,

Table 4 Pearson correlation coefficients (R) and COD values between MCM3.3.1 and URMELL, JAMv2b and RACM for the remote summer case with full radiation as well as for the sensitivity run comprising all discussed anthropogenic and isoprene-related modifications (case 5)

		URMELL		JAMv2b		RACM		URMELL sens	
Scenario	Compound	R	COD	R	COD	R	COD	R	COD
rem_s_1	O_3	0.881	0.071	0.998	0.010	0.986	0.115	0.985	0.077
	NO	0.982	0.159	0.986	0.137	0.971	0.137	0.981	0.129
	NO_2	0.980	0.184	0.987	0.084	0.972	0.100	0.992	0.065
	OH	0.987	0.340	0.998	0.104	0.987	0.065	0.997	0.120
	HO_2	0.990	0.345	0.991	0.372	0.998	0.229	0.989	0.336
	H_2O_2	0.992	0.185	0.995	0.041	0.997	0.146	0.989	0.045
	NO_3	0.954	0.379	0.986	0.202	0.967	0.448	0.973	0.161
	HNO_3	0.959	0.278	0.759	0.503	0.988	0.104	0.999	0.079
	HCHO	0.959	0.048	0.993	0.116	0.964	0.304	0.993	0.154
	PAN	0.998	0.037	0.999	0.105	0.999	0.332	0.998	0.211
	GLY	0.472	0.202	0.628	0.578	0.615	0.547	0.530	0.463
	MGLY	0.892	0.114	0.843	0.371	0.891	0.684	0.792	0.337
	C_5H_8	0.892	0.333	0.989	0.072	0.990	0.036	0.989	0.082
	MACR	0.519	0.268	0.980	0.193	0.995	0.197	0.963	0.219
	MVK	0.711	0.223	0.757	0.492	0.999	0.149	0.780	0.471
	HCOOH	0.952	0.329	0.998	0.083	0.972	0.364	0.994	0.113
	CH_3O_2	0.952	0.192	0.959	0.419	0.956	0.382	0.934	0.463
	$CH_3C(O)O_2$	0.982	0.204	0.985	0.281	0.984	0.198	0.990	0.293
	CH_3COOOH	0.999	0.116	0.999	0.178	0.988	0.299	0.999	0.131
	CH_3COCH_2OH	0.997	0.079	1.000	0.273	0.998	0.103	1.000	0.090

NO_2, NO_3 and HO_2 concentrations decreases. This is also the case for the winter scenarios, but NO and NO_2 estimates increase for all reduced mechanisms (Fig. S2-6 and S2-7†). In general, nearly all correlation coefficients of URMELL are above 0.8 (Table S2-1†) for the winter scenarios (Fig S2-6 and S2-7†). Here, the weaker photochemical activity and lower temperature reduce the diurnal variability, straightening most temporal profile, whereby the curve similarity increases. For MGLY, URMELL predicts very similar curves to the MCM3.3.1 for all scenarios (see Fig. 2o and S2-3o–S2-7o†).

All mechanisms show similar diurnal isoprene cycles (Fig. 2d). The increase in daytime OH lowers the isoprene minimum and causes a slightly earlier onset of afternoon isoprene rise for URMELL, which impacts the correlation and COD values (Table 4). This also holds for the rem_05_s case (Fig. S2-5d†). For the winter scenarios (Fig. S2-6d and S2-7d†), the OH concentration is much lower and only present for a shorter period of time which minimizes this shift and leads to higher R values ($R > 0.9$). For the isoprene reaction products MACR and MVK, stronger diurnal fluctuations are visible compared to all other mechanisms (Fig. 2h and l). This is caused by higher production from isoprene chemistry while at the same time degradation is intensified due to higher oxidant concentrations. But these variations attenuate for reduced actinic radiation and the winter scenarios (Fig. S2-5h/l–S2-7h/l†). MACR is linked to $ISOPDO_2$ and MVK to $ISOPBO_2$. For the rem_1_s scenario, MVK and MACR are directly impacted by the ISOPOO composition. In JAMv2b the reaction of C_5H_8 with OH yields 0.4/0.35/0.25 $LISOPACO_2$/$ISOPBO_2$/$ISOPDO_2$ and in URMELL 0.05/0.6/0.35, respectively. Thus, higher MVK and similar MACR values are simulated. But, the increased oxidant concentration (Fig. 2a, e and j) intensifies the degradation. When reducing OH, MCM3.3.1 and URMELL adjust in the case of the rem_05_s scenario, while for the winter scenario URMELL simulates higher concentrations. Besides MACR and MVK, HCHO is *e.g.* linked to $ISOPBO_2$ and $ISOPDO_2$ chemistry. The simulated diurnal cycles for the rem_1_s scenario are similar for all mechanisms (Fig. 2c), but URMELL produces higher concentrations. For reduced photolysis and lower temperatures (Fig. S2-5d and S2-7d†) the impact of the ISOPOO pool composition manifest in even higher HCHO concentrations. CH_3COCH_2OH is on the other hand mainly produced from $LISOPACO_2$. Therefore, due to the much lower $LISOPACO_2$ production yield in URMELL lower CH_3COCH_2OH concentrations compared to JAMv2b are simulated.

Peroxy radical concentrations of CH_3O_2 and especially of $CH_3C(O)O_2$ are lower for all mechanisms compared to the MCM3.3.1 (Fig. 2q/r and S2-5q/r–S2-7q/r†). Important sources for both radicals are *e.g.* photolysis processes, ozonolysis reactions and for CH_3O_2 also $CH_3C(O)O_2$ reaction pathways. The $CH_3C(O)O_2$ offset between the MCM3.3.1 and the other mechanisms increases for the rem_05_s and the winter scenarios and is caused by changes to ozonolysis processes and the ISOPOO pool. This reduction in $CH_3C(O)O_2$ also lowers PAN (Fig. 2g and S2-5g–S2-7g†) and CH_3COOOH (Fig. 2s and S2-5s–S2-7s†) but compared to JAMv2b PAN is slightly reduced due to slower k_{NO_2} and CH_3COOOH enhanced due to faster k_{HO_2} reaction rate coefficient. With reduced photolysis and $CH_3C(O)O_2$ availability, day-time CH_3O_2 production shrinks. Night-time CH_3O_2 production is governed by ozonolysis processes. The higher CH_3O_2 yield from $C_5H_8 + O_3$ oxidation and fast reaction rate coefficient generates a still partly increasing night-time trend for URMELL while the MCM3.3.1 predicts a fast increase (also see Sect. 4.1, 4.3) followed by a continuous decrease. This is

producing opposing trends and results in low or even negative R values (Table S2-1†).

For GLY (Fig. 2k), the deviation from the diurnal cycle proposed by MCM3.3.1 is of specific interest and reveals low correlation values. URMELL simulates a minimum at 6:00, a maximum at 15:00, followed by a decrease until 19:00, after which somehow stable concentrations are reached (slightly increasing) until 5:00. The rather low GLY + NO_3 reaction constant of URMELL hinders night-time GLY degradation (Fig. 2k). But compared to the MCM3.3.1, night-time URMELL GLY production from isoprene channels are much lower (Sect. S2.3.4†). The MCM3.3.1 simulates maximum GLY concentration around 6:00. URMELL shows a stronger day-time production mainly linked to newly implemented C_5H_8 chemistry (MVK, ISOPOO pool) with a strong photolysis component. Whereas the MCM3.3.1 simulates only minor day-time GLY production resulting in a saddle point instead of a maximum followed by a minimum at 19:00. Maximum concentrations of GLY coincide with minimum C_5H_8 concentrations confirming a link to C_5H_8 daytime chemistry, which is dominated by OH chemistry. In the cases of reduced actinic radiation (Fig. S2-5k†), GLY is negatively correlated. Now, the day-time GLY production of the MCM3.3.1 cannot outcompete the consumption, while URMELL still predicts a small increase. These opposing trends invoke a slightly negative $R = -0.051$ value. For the winter scenarios (Fig. S2-6k and S2-7k†), ozonolysis dominates for both scenarios, but with much higher production for the MCM3.3.1 ($R = 0.9$).

The increase in OH also boost day-time HNO_3 formation *via* NO_2 reaction (Fig. 2n) resulting in a clear diurnal cycle for the rem_1_s case. But with attenuating OH concentrations for the other scenarios this HNO_3 day-time production diminishes. For HCOOH (Fig. 2p and S2-5p–S2-7p†), URMELL has a stronger day-time component and shows a clear diurnal cycle for the summer cases. Changes to HCOOH are mainly caused by the different treatment of the stabilized Criegee intermediate CH_2OO (see Sect. 2.2.1) and changes to ozonolysis reactions especially for the reaction of MVK + O_3. Measurements from remote high HO_x and isoprene rich locations would support stronger day-time production strength of GLY, HCOOH, and HNO_3 resulting in distinguishable diurnal cycles as simulated with URMELL.[81,82,118,121] Changes to the abundance of these compounds alters the atmospheric oxidant budget mainly through their strong linkages to OH, HO_2, RO_2 and O_3. GLY and HNO3 are additionally.

In conclusion, URMELL simulates concentration time series of various species in remote environments for different radiation and temperature regimes in the same manner as the benchmark MCM3.3.1 ($R > 0.9$ for most substances, but with partly higher COD values, Table 4). Overall, URMELL predicts a much higher remote tropospheric oxidative capacity. When resetting all mentioned updates (Table 3, case 5), O_3, NO, NO_2, NO_3, OH, HO_2 concentration time series are, of course in better accordance with JAMv2b, in most cases even closer to the MCM3.3.1 with excellent correlation ($R > 0.98$) and low COD values (Table 4). Moreover, for compounds (*e.g.* H_2O_2, NO_3, HNO_3) directly linked to the oxidants a close match to the MCM3.3.1 is reached.

The MCM3.3.1 contains more than 5500 species and OH is the dominant oxidizing agent for most non-radical species. Therefore, the MCM3.3.1 provides numerous additional OH sinks, not included in URMELL. Hence, further extension for example of the monoterpene chemistry might reduce the higher predicted concentration of OH and O_3 in remote areas. Still, measurements in rural regions of the tropical forest support higher O_3 and OH concentrations in isoprene-dominated regimes, even though this is currently a controversy and subject of recent scientific discussion.[9,117,120] Therefore, CTMs that do not take these updates into account might not be able to predict concentrations comparable to ambient values in isoprene-dominated environments, such as the Amazonian rain forest.

4.3 Urban case

Fig. 3 illustrates the modeled concentrations of key gas-phase compounds for the urb_s_1 scenario (no attenuated actinic radiation) for all mechanisms. In addition, Table 5 shows all Pearson correlation coefficients (R) and COD values calculated between MCM3.3.1 and the other non-explicit mechanisms for the urb_s_1 scenario. The plots and tables for the other scenarios are provided in the ESI (Fig. S2-2 till S2-4 and Table S2-1).†

The correlation values improved for nearly all species for the summer cases when comparing JAMv2b and URMELL with the MCM3.3.1 (Table 5 and S2-1†). In comparison with the MCMv3.3.1, all reduced mechanisms are able to reproduce the

Table 5 Pearson correlation coefficients (R) and COD values between MCM3.3.1 and URMELL, JAMv2b and RACM for the urban summer case with clear sky conditions. Bold numbers highlight highest R values indicating best representation of MCM3.3.1 concentration trends and lowest COD for closest MCM3.3.1 approximation

		URMELL		JAMv2b		RACM	
Scenario	Compound	R	COD	R	COD	R	COD
urb_s_1	O_3	**0.999**	**0.012**	0.987	0.064	0.994	0.014
	NO	**0.998**	**0.076**	0.958	0.169	**0.999**	0.080
	NO_2	**0.999**	**0.067**	0.916	0.126	0.975	**0.058**
	OH	**0.998**	0.290	0.953	**0.148**	0.995	0.200
	HO_2	**0.999**	**0.235**	0.944	0.407	0.996	0.324
	H_2O_2	**1.000**	**0.105**	0.989	0.235	0.998	**0.063**
	NO_3	**0.996**	0.055	0.959	**0.175**	0.968	0.179
	HNO_3	**0.725**	**0.063**	0.190	0.104	0.488	**0.037**
	HCHO	**0.999**	**0.024**	0.956	0.150	0.987	0.193
	PAN	**1.000**	**0.065**	0.999	0.085	**1.000**	0.122
	GLY	**0.965**	**0.082**	−0.517	0.642	0.229	0.134
	MGLY	**0.982**	**0.131**	0.796	0.212	0.945	0.517
	C_5H_8	**0.964**	**0.104**	0.924	0.107	0.871	0.179
	MACR	0.911	**0.090**	**0.929**	0.189	0.919	**0.088**
	MVK	**0.890**	**0.121**	0.411	0.309	**0.899**	0.232
	HCOOH	0.925	0.476	**1.000**	**0.118**	0.995	0.285
	CH_3O_2	**0.833**	**0.304**	0.809	0.480	**0.864**	**0.158**
	$CH_3C(O)O_2$	**0.999**	**0.070**	0.972	0.257	0.986	0.231
	CH_3COOOH	**0.999**	**0.317**	0.994	0.325	0.994	**0.101**
	CH_3COCH_2OH	0.991	0.175	**0.996**	**0.099**	0.994	0.215

modeled cycle of the most frequently measured air quality components such as O_3, NO and NO_2 for clear sky conditions (Fig. 3) as well as OH, H_2O_2, NO_3, HCHO, PAN, HCOOH, $CH_3C(O)O_2$, CH_3COOOH and CH_3COCH_2OH with correlation values above 0.9. However, RACM and JAMv2b show deficits for HNO_3 and GLY leading to lower or even negative correlation values. Even though, correlation values are high for most species, the magnitudes of certain species differ between the mechanisms. URMELL provides up to 50% higher peak HO_y (H_2O_2, OH, HO_2) concentrations than all other mechanisms. Based on performed sensitivity studies presented before (Sect. 4.1 and S2.2†), this difference is mainly linked to changes in $RC(O)O_2$, isoprene chemistry and photolysis processes (same reactions as indicated for the sensitivity studies in Sect. 4.1 and listed in Tables S1-2 and S1-3† apply, therefore similar results occur). All reduced mechanisms tend to overestimate night time NO_3 but URMELL shows the largest similarity to the MCM3.3.1 with R being greater than 0.99 for all summer scenarios (Tables 5 and S2-1†). Importantly, the diurnal cycle of GLY and HNO_3 modeled by the MCM3.3.1 is reproduced by URMELL, only. For HCHO and MGLY, very similar concentrations are modeled with URMELL together with high *R* and low COD values. The highest deviation from the MCM3.3.1 is evident for HCOOH which is primarily caused by the changed Criegee intermediate treatment of the CH_2OO biradical (see Sect. 2.2.1 for further details). As the only CH_3COOOH source is the reaction of $CH_3C(O)O_2$ with HO_2, the higher CH_3COOOH with URMELL are caused by the faster production and the much slower degradation by OH. Higher night-time CH_3O_2 concentrations modeled with the MCM3.3.1 are due to ozonolysis reactions.

This becomes even more evident for the winter scenarios (Fig S2-3q and S2-4q†), when photolysis processes are insignificant loss processes and ozonolysis reactions gain in importance. Further investigation of the modeled CH_3O_2 concentration by the MCM3.3.1 revealed additional sources (*e.g.* CH_3CHOOA, CH_3CHOOB, CH_3CHOOC) from alkene ozonolysis. But based on Cox *et al.*[73] the degradation channels of Criegee intermediates have much lower CH_3O_2 production rates. As for the ozonolysis of C_3H_6 which does not include a direct CH_3O_2 pathway (see Sect. 2.2) but in the MCM3.3.1 would initiate the production of CH_3CHOOA. Furthermore, in JAMv2b most alkenes are lumped into BIGENE, for which no reaction with O_3 is implemented and therefore, no CH_3CHOOB and CH_3CHOOC formation is considered. Here, more knowledge is needed to adjust the representation of alkenes in URMELL, including the lumping and adequate reaction equations. However, this is out of scope of this study, it will be the focus of further mechanism development. Ozonolysis reactions are also a major night-time HO_2 source. While during summer, HO_2 would peak around noon, in winter the night-time HO_2 ozonolysis peak exceeds the day-time peak for the MCM3.3.1 (Fig. S2-3i and S2-4i†). For URMELL, the night-time peak is much lower compared to the MCM3.3.1 and for the urb_w_05 scenario even lower than the day-time peak.

The high NO_x concentrations of the urban scenarios result in HO_x limit regimes, which makes the winter scenarios highly sensitive to any kind of HO_x changes. As the HO_x and NO_x cycling is linked to O_3, it is impacted, too. Furthermore, the reduction in CH_3O_2 and HO_2 boost O_3 (Fig. S2-3a and S2-4a†) and NO_3 (Fig. S2-3j and S2-4j†) night-time oxidation which decrease their concentrations and in turn enhances NO_x (Fig. S2-3b/f, S2-4b/f†). The stronger O_3 depletion especially for the urb_w_05 scenario also causes a shift towards $CH_3C(O)O_2$ degradation channels resulting into reduced $CH_3C(O)O_2$ concentrations (Fig. S2-3r and S2-4r†). Nevertheless, compared to JAMv2b URMELL still provides better R and COD values for both winter scenarios (Table S2-1†).

The intensified NO_3 oxidation for the urb_05_w scenario also highlights the importance of the NO_3 reaction with mono-hydroxy phenols. This reaction produces ring-opening products with an ON(=O)=O group ($NPHENOLO_2$, $NCRESO_2$) for which various approximations are available and a sensitivity study testing the different approaches is presented in the ESI (S2.2†).

5 CTM results

For the CTM simulation, similar results as with the well-established mechanism RACM are desired, when comparing with NO, NO_2 and O_3 measurements. To analyze the model data of these three compounds, 62 measurement sites are selected throughout Germany comprising a variety of different VOC and NO_x regimes. Due to data gaps or episodes of constant values when the detection limit of the measurement device is reached, only 57 stations are considered for the comparisons. These include 24 remote background (BR), 14 urban background (BU), 8 traffic (T) and 11 industrial/traffic and industrial (IR/IU/TI) sites. While for nearly all stations O_3 data is available, NO_2 and NO data is limited to 40 and 14 stations, respectively. An overview of the sites is provided in Table S3-1† and a map containing all measurement sites is given in Fig. S3-1b.†

Note, that the accuracy of the different simulated time series depend on multiple factors, such as quality of anthropogenic and biogenic emission fields, orographic effects, deposition processes, meteorological parameters which influence the dispersion and boundary layer height, and not primarily on the applied chemical mechanism. Another very important aspect is the model resolution, as a grid cell typically comprises multiple land use categories and/or structures. Especially in cities, buildings or other obstacles influence the transport of airborne substances such as air pollutants resulting in accumulation and removal areas. Also transition areas between, for example, cities and natural vegetation holds some uncertainties with regard to exactly predicting concentrations at a specific point. Additionally, local deviation from the standard emission profile used to calculate the emissions are hard to capture. Furthermore, the highly temporal fluctuation of measurements is often more pronounced compared to model predictions. Therefore, multiple aspects have to be considered when analyzing time series of modeled and measured data. To reduce measurement noise and to compensate outliers (extreme events, special events *etc.*) also the average diurnal concentration cycles for May 2014 are calculated. Please also note, that the obtained mechanistic differences presented in Sect. 4.1 cannot be directly transferred to the CTM simulations as emissions and

meteorological conditions change with space and time. Therefore, the high increases in OH and ozone as seen from the remote case studies above are not presumed.

Table S3-2† summarizes the minimum, mean, maximum and standard deviation for all measurements and model simulation time series of O_3, NO_2 and NO, as well as the associated correlation and COD values between the measurement and model simulations for the selected stations. Both RACM and URMELL predict quite similar concentration time series with correlation and COD values in the range of 0.1 of each other for most stations. In the case of O_3, correlation values are above 0.5 for all stations. When looking at the entire time series, RACM provides more often slightly higher correlation (25 out of 56 for O_3, 20 out of 40 for NO_2, 11 out of 14 for NO) and almost always slightly lower COD values. Note that for R_{RACM}–R_{URMELL}<0.01 both time series are considered too similar to count for either mechanism (R_{RACM}–R_{URMELL}<0.01 16, 9 and 2 times, respectively) and are indicated by yellow coloring in Fig S3-1b.† However, average diurnal concentration cycles provide more often (21, 18, 0 and R_{RACM}–R_{URMELL} <0.01 25, 9 and 6 times, respectively) closer agreement to the measurements with correlation values for O_3 of 0.8 or higher (Table S3-3†) for URMELL. In Fig. S3-1b,† the color indicates if RACM (red) or URMELL (green) provides higher correlation values with O_3 measurements. This will be further elaborated within in the next subsection.

5.1 Remote sites

For the remote sites, only O_3 is further evaluated, because of the lack of NO_x data. In the north east of the domain, a cluster where RACM gives better O_3 correlation values for remote sites (Fig. S3-1b†) is evident. Further investigations indicate a link between the O_3 cycles and the land use type, *e.g.* different tree species. Therefore, measurement sites within or close to forests of the four most common German tree species are investigated further: Spreewald (pine; Fig. S3.2-1 and S3.2-5†), Kellerwald (beech; Fig. S3.2-2 and S3.2-6†), Simmerath (oak; Fig. S3.2-3 and S3.2-7†) and Schmuecke (spruce; Fig. S3-4 and S3-8†). A brief description of the BVOC emissions is given in the ESI S.3.2.1† (a more detailed description of the implemented BVOC emission algorithm can be found in Luttkus *et al.*[4]). Especially in the east, continuous pine induced monoterpene and the lack of pine isoprene emissions invoke *e.g.* slightly lower correlation values for URMELL. This also holds for urban stations within monoterpene dominated areas. Whereas in isoprene, OVOC and synthesis monoterpene emission dominated regions (oak, beech, spruce, mixed forest) similar or higher correlation values occur (Fig. S3-1b†).

The time series (Fig. 4, 5 and S3.2-1–S3.2-4†) indicate an intense O_3 episode from the 19th until the 23rd of May 2014. During this episode calm winds, high solar radiation and warm temperatures boost BVOC emissions and facilitate local degradation processes. Both RACM and URMELL underestimate this O_3 episode for all stations. Possible reasons for the underestimated ozone concentration are: (i) under predicted BVOC emissions, (ii) location at higher altitude (which is the case for all spruce forest within the lower mountain range) which impacts several terrain related factors, *e.g.*, stratospheric ozone intrusion, meteorological parameters (wind speed, wind direction, atmospheric stability, planetary boundary layer height). Especially during this episode, large deviation between RACM and URMELL are modeled for spruce, beech and mixed forests. Here URMELL predicts higher night-time O_3 concentrations which are in better agreement with the measurements (Fig. 4, S3.2-2 and S3.2-4†) and result in higher correlation values (all green dots in Fig. S3-1b†). The O_3 increase for spruce is so high (Fig. S3.2-4†), that a complete offset between measured and modeled O_3 concentration is observed, which needs to be further investigated.

5.2 Urban sites

For the urban stations (squares and triangles), 13 (7) out of 32 stations show better correlations for the mean diurnal O_3 cycle with URMELL and 16 (11) with similar values (entire time series). All three stations with worse correlations are within the north east of Germany again. In general, URMELL produces a slower O_3 decay after approximately 18 UTC until midnight resulting in higher O_3 concentrations during the first half of the night (exemplary see Fig. 5). However, minimum O_3 concentration between 4 and 6 UTC is often lower in the model due to

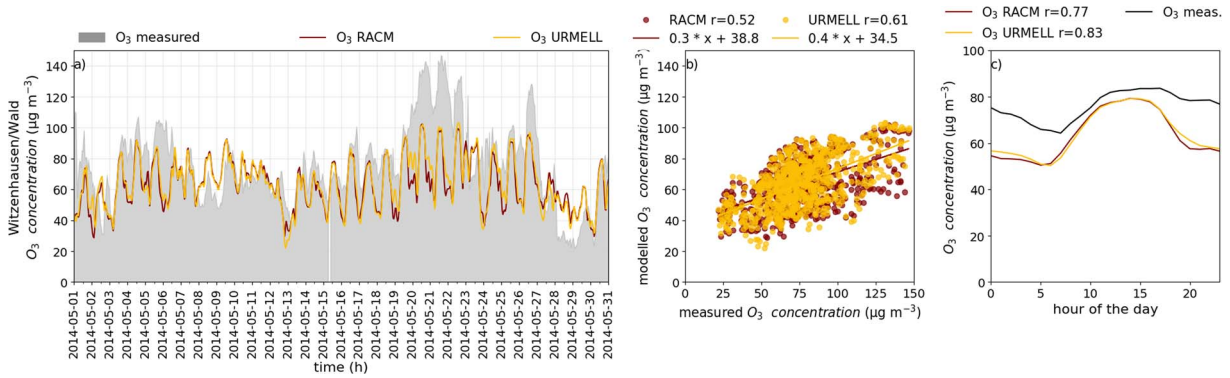

Fig. 4 Time series of O_3 in (a)–(c) for Witzenhausen (mixed forest); measurements in grey for (a), black line for (c) as well as modeled concentrations using RACM (red line) and URMELL (yellow line).

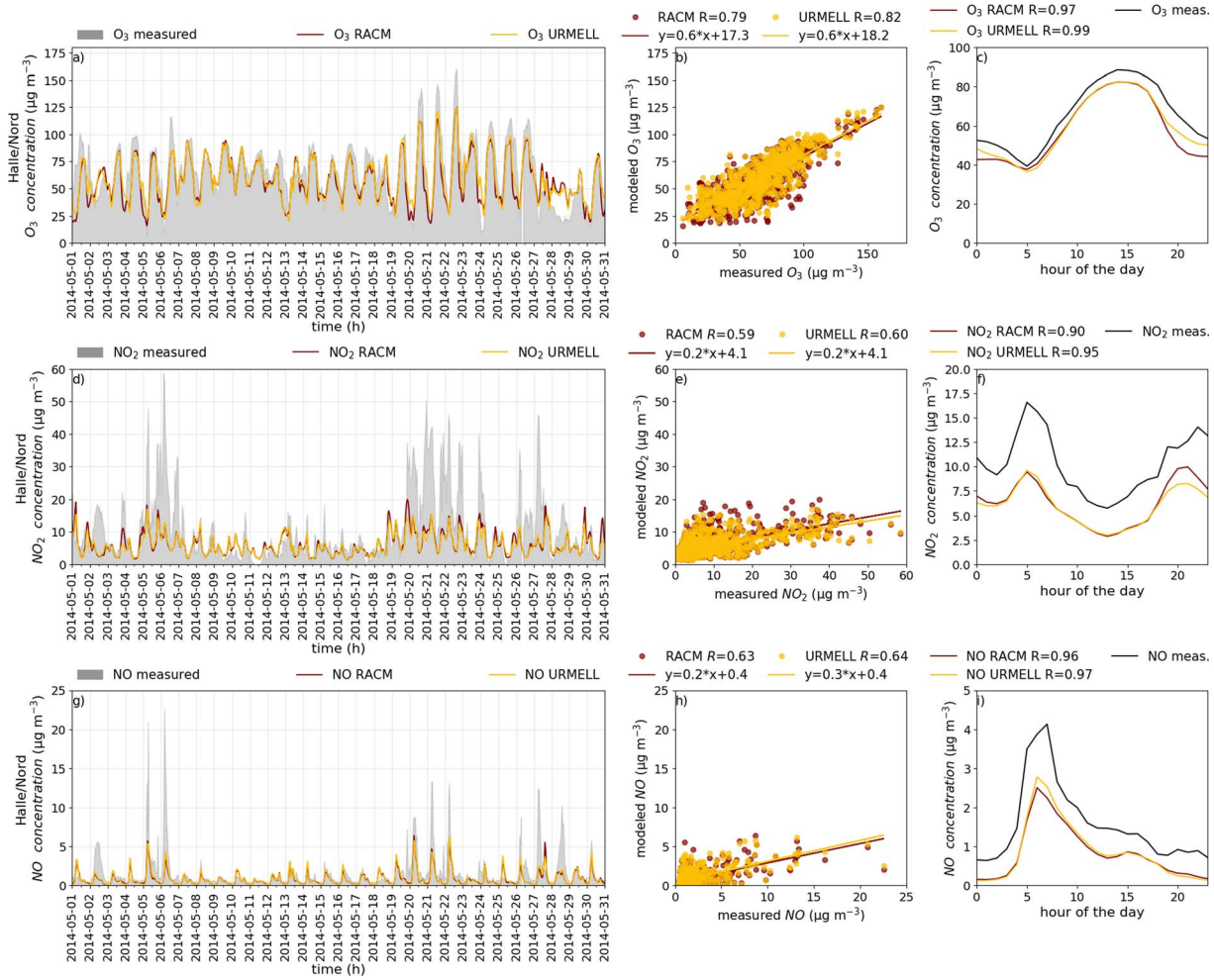

Fig. 5 Time series of O_3 in (a)–(c); of NO_2 in (d)–(f); of NO in (g)–(i) for Halle/Nord measurements in grey for (a), (d) and (g) black line otherwise as well as modeled concentrations using RACM (red line) and URMELL (yellow line).

faster and/or prolonged decay due to enhanced NO concentrations. Maximum concentrations are similar. The diurnal NO_2 cycle shows two peaks one around 5 UTC and a second one around 20 UTC. For the first peak, similar or slightly increased concentration are reached for URMELL, while for the second NO_2 peak URMELL generally produces lower concentrations. These changes can be mainly attributed to $RC(O)O_2$ changes. For most sites, this change in NO_2 peak concentrations better reproduce the measured data. But in cases where measurements have a higher second peak, RACM has higher correlation values (see Table S3-2†). For NO, there is no clear differentiation between RACM and URMELL possible. All stations show a clear peak around 6 UTC, but depending on the sites, sometimes RACM and sometimes URMELL shows higher/lower concentrations and may produce a second smaller NO peak in the afternoon. Additionally, due to the limited amount of data, no definite trend can be derived.

5.3 Spatial (O_3) concentration distribution on May 20th

To further elaborate the deviation during the O_3 episode, O_3 map plots for 3 UTC, 13 UTC and 19 UTC of the 20th of May are presented. This allows insights into the spatial distribution of the identified simulated O_3 deviation. Due to the interwoven links between HO_x, NO_x, O_3, isoprene and monoterpenes, an assessment of purely individual impacts is not feasible.

At 3 UTC, highest O_3 concentrations are reached for beech- and spruce-dominated areas independent of the chemical mechanism. However, URMELL simulates higher O_3 concentrations (Fig. 6) for most of the domain compared to RACM. In lower NO_x environments (Fig. S4-1†), highest OH and monoterpene concentrations are reached with URMELL for pine (Fig. S4-2 and S4-3†).

At 13 UTC, URMELL mainly predicts lower OH concentration, but in pine dominated areas a certain fraction of higher OH concentration occurs. Monoterpene concentrations are highest for beech followed by pine with URMELL. Here, pine emit high quantities of APIN while beech emit BPIN with individual degradation pathways, whereas in RACM both are treated as API. Furthermore, the strong OVOC emissions of beech support the changes to the OVOC emission split including the treatment of various individual species and their chemistry. The new OVOC as well as monoterpene treatment is essentially

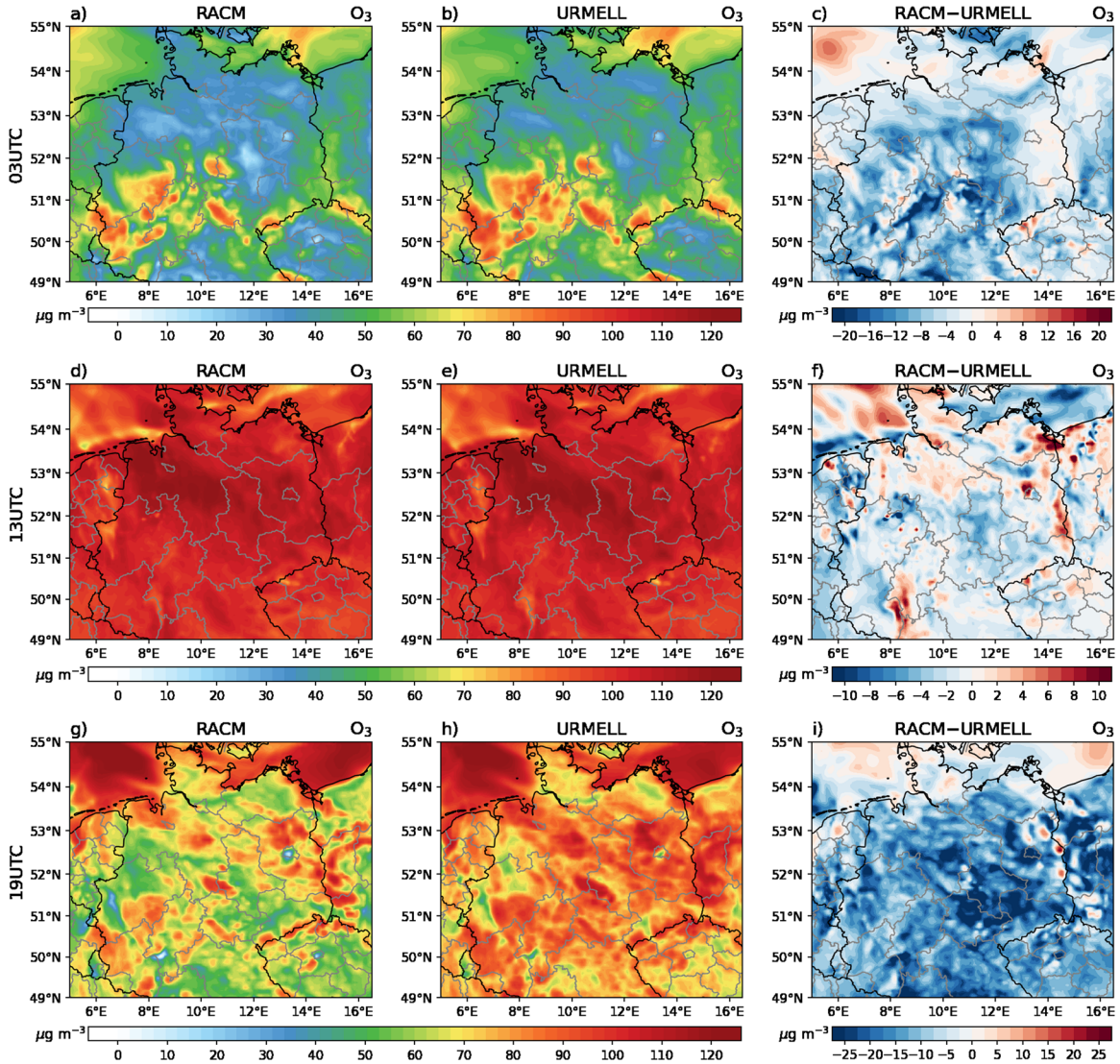

Fig. 6 Ozone concentration for the 20th of May 2014 at 3 UTC (a–c)), 13 UTC (d–f) and 19 UTC (g–i) for RACM (a, d and g), URMELL (b, e and h) and the difference between RACM and URMEL (c, f and i).

involved in OH and O_3 concentration degradation processes. Isoprene emission is rather low for most parts, but gain in importance for oaks (Fig. S3.2-3 and S3.2-7†). Unfortunately, oaks often coincide with high NO_x and monoterpene emissions, which limits the localization of isoprene dominated regimes where changes described in Sect. 4.1 could be identified. One area of isoprene-dominated chemistry could be clearly identified (red circled area in Fig. 3a). Here, the differential plot of isoprene (Fig. S4-4f†) indicates lower concentrations with URMELL while at the same time OH (Fig. S4-2f†) and O_3 (Fig. 6f) values are higher. The enhanced oxidant concentrations also boost monoterpene degradation resulting in lower concentration values with URMELL (Fig. S4-3f†). For higher NO_x concentrations, higher NO and NO_2 (Fig. S4-1f†) values result in lower O_3 concentration and *vice versa*, independent of the higher isoprene concentrations simulated with URMELL (see blue areas in the Netherlands and north of Berlin of Fig. S4-4f†).

At 19 UTC, pine forests become discernible in the O_3 plot (Fig. 6), but again with higher values for URMELL due to a slower O_3 decay. Monoterpene concentrations remain higher for beech, while much lower concentrations are reached for pine in combination with lower OH values than for beech-dominated areas. For further investigation of the monoterpene-related impacts, more knowledge about the individual monoterpenes is required.

6 Summary and outlook

In this study, we presented the new chemical mechanism URMELL, which was developed for better representation of the atmospheric chemistry of anthropogenic as well as biogenic VOCs in atmospheric models aiming at advanced air quality assessments and direct and explicit SOA modelling. The focus of the URMELL development was on isoprene and aromatics, as

they are strongly linked to the budget of key pollutants and oxidants, such as O_3, NO_x and HO_x.

Originating from JAMv2b *e.g.*, photolysis rates, certain reaction rate constants, the ozonolysis of ethene and propene, the treatment of $RC(O)O_2$, aromatics, sesquiterpenes and isoprene were updated and extended. The impact of these changes was analyzed for specific gas-phase compounds under various meteorological conditions in urban and remote environments using the box model SPACCIM. In the analyses, compound concentrations predicted by the reduced gas-phase mechanisms JAMv2b, RACM or the near explicit mechanism MCM3.3.1 were compared with URMELL. For all urban scenarios, URMELL produces high correlation values above (or close to) 0.8 for most compounds compared to the MCM3.3.1. For the remote scenarios, URMELL simulates much higher oxidant concentrations than all other mechanisms. Based on performed sensitivity studies, approximately half of the increase can be addressed to non-isoprene (mainly photolysis and $RC(O)O_2$) and the other half to isoprene-related mechanism changes. These adjustments in URMELL may help to overcome the recent shortage in the modeled HO_x budget compared to measurements. Furthermore, the model performance is also improved for not so commonly studied compounds, such as glyoxal or methylglyoxal, due to better depiction of their diurnal cycles. From these box model analyses, it was possible to identify several aspects that require further investigation and more knowledge. The most relevant non-isoprene related aspects are: (i) formic acid gas-phase formation pathways, (ii) stable Criegee intermediate chemistry, (iii) verification of the degradation of aromatic ring-opening radicals with an ON(=O)=O group, (iv) alkene ozonolysis and (v) monoterpene treatment.

Even though a lot of research has been done on isoprene during the last decade, there are still uncertainties. For example, no explicit recommendation exists for ISOPOO pool composition. So far there is a multitude of varying yields for the complex C_5H_8 + OH chemistry applied in reduced chemical mechanisms. But, these ratios are crucial as they control the production of the most important reaction products MACR, MVK and HPALDs. Furthermore, the ISOPOO pool also determines the HO_x recycling ability through H-shift reactions and, as the implementation of these H-shift reactions significantly increases the HO_x concentration, but the rate constants need to be further determined.

URMELL has further been successfully applied in the chemical transport model COSMO-MUSCAT with good results in both urban and rural environments. Time series comparisons for O_3 and NO_2 confirm a good agreement between RACM and URMELL with correlation and COD values in close approximation (0.1 of each other). While RACM predicts slightly better correlation values for pine, URMELL better predicts O_3 concentration during intense O_3 episodes for OVOC, light-dependent monoterpene and isoprene emission dominated regions. A slower O_3 decay and a lower NO_2 peak are identified post meridiem for remote low NO_x environments. This improves the model performance for most remote non-pine stations compared to RACM. A complete offset between measured and modeled O_3 concentration is observed in spruce-dominated areas, which certainly requires further investigation. No improvement has been achieved for low isoprene emitting environments, such as pine forests. This also transfers to urban environments in isoprene-limited regions. The updates to anthropogenic chemistry improved the correlation values of the mean daily concentration cycles for urban and traffic sites not just for O_3 but also for NO_2. Therefore, URMELL is capable of predicting gas-phase concentrations of the air pollutants in urban and remote environments for different temperature and radiation regimes. As URMELL is designed to also enable direct and explicit SOA formation, it can be considered a suitable tool for simulating regional air quality in a changing atmosphere, because of the more sophisticated description of NMVOC oxidation compared to RACM.

Especially during stable, warm and sunny conditions, URMELL simulates higher O_3 night-time concentrations than RACM, which reduces the offset between measured and modeled values. However, O_3 maximum concentrations are still not reached mainly in monoterpene-dominated regimes, which could be related to the incomplete monoterpene oxidation schemes. The analyses allow to suggest a tree species dependent O_3 cycle, but to verify this hypothesis additional research is needed. This includes the continuing development of more detailed chemical mechanisms capable of treating a variety of BVOCs including diverse monoterpenes, which are dominating the BVOC composition in coniferous forests.

Overall, it has to be noted that URMELL provides similar NO_x and O_3 concentration time series for all urban box model simulations compared to the MCM3.3.1 and RACM. However, the better agreement of frequently produced organic reaction products such as HCHO, GLY and MGLY of URMELL with the MCM3.3.1 indicates improved chemical degradation schemes. The improved isoprene HO_x recycling in remote environments raise OH concentrations to the range of measured values ($\sim 10^6$ molecules per cm^3). Furthermore, in CTM simulations URMELL produces similar O_3 and NO_x concentrations to RACM with slightly higher correlation values for urban and non-monoterpene-dominated areas. In addition, the integration of highly oxidized reaction products produces a much higher variety of species in URMELL and suggest a direct and explicit SOA formation potential. This will be addressed further in a follow-up study. Next to the anthropogenic and isoprene adjustments we want to emphasis the changes to $RC(O)O_2$, especially the reaction rate constant k_{NO_2}.

A better understanding of the impact of specific characteristics of individual tree species on atmospheric chemistry is key for a livable future as many trees have been and are being planted in both urban and rural areas as part of re- and afforestation programs for climate adaptation and mitigation measures. As a warming climate is likely to increase BVOC emissions, their importance on atmospheric chemistry advances. Therefore, there is an urgent need to expand the knowledge on BVOC chemical degradation such as: (i) the identification of significant deviations between the reaction pathways of individual BVOCs within OVOCs and monoterpene clusters, (ii) the differentiation of the BVOC diversity in

chemistry mechanisms and (iii) the formation of stable accretion products (ROOR) from the reaction between two peroxy radicals for varying BVOCs, as they are important SOA sources.

Despite mechanism development, there is also an essential demand for comprehensive and time-resolved measurements, particularly of VOCs and OVOCs, over long-time periods and vast spatial coverage to further evaluate model results. This is especially true for yet not so frequently measured substances such as formaldehyde, glyoxal, methylglyoxal and formic acid. Measurements of their main BVOC precursors, isoprene and the most common monoterpenes, would additionally help to constrain BVOC emission parameterizations in models and possibly help to identify stress induced BVOC emissions, such as under heat and drought conditions which alters the BVOC emission strength and composition. As heat and drought are predicted to increase in frequency and intensity with progressing climate warming in many regions such as Central Europe, possible feedback mechanisms can only be evaluated with a comprehensive chemical mechanism still applicable in chemical transport and climate models.

Author contributions

Conceptualization: MLL, RW, AT, EHH. Data curation: MLL. Formal Analysis: MLL. Funding acquisition: MLL. Investigation: MLL. Methodology: MLL, RW, AT, EHH. Project administration: MLL, RW. Software: MLL, RW. Supervision: MLL, RW. Validation: MLL. Visualization: MLL. Writing – original draft: MLL. Writing – review & editing: MLL, EHH, AT, RW, HH, IT.

Conflicts of interest

There are no conflicts to declare.

Acknowledgements

This work was funded by the PhD scholarship of the German Federal Environmental Foundation (Deutsche Bundesstiftung Umwelt, DBU) granted to MLL (AZ 20016/452). We thank the German Environment Agency (Umweltbundesamt - UBA) for the access to the measurement data.

References

1 G. Curci, M. Beekmann, R. Vautard, G. Smiatek, R. Steinbrecher, J. Theloke and R. Friedrich, Modelling study of the impact of isoprene and terpene biogenic emissions on European ozone levels, *Atmos. Environ.*, 2009, **43**, 1444–1455.

2 O. J. Squire, A. T. Archibald, P. T. Griffiths, M. E. Jenkin, D. Smith and J. A. Pyle, Influence of isoprene chemical mechanism on modelled changes in tropospheric ozone due to climate and land use over the 21st century, *Atmos. Chem. Phys.*, 2015, **15**, 5123–5143.

3 K. N. Sartelet, F. Couvidat, C. Seigneur and Y. Roustan, Impact of biogenic emissions on air quality over Europe and North America, *Atmos. Environ.*, 2012, **53**, 131–141.

4 M. L. Luttkus, E. H. Hoffmann, L. Poulain, A. Tilgner and R. Wolke, The Effect of Land Use Classification on the Gas-Phase and Particle Composition of the Troposphere: Tree Species Versus Forest Type Information, *J. Geophys. Res.: Atmos.*, 2022, **127**, e2021JD035305.

5 M. Kanakidou, J. H. Seinfeld, S. N. Pandis, I. Barnes, F. J. Dentener, M. C. Facchini, R. V. Dingenen, B. Ervens, A. Nenes, C. J. Nielsen, E. Swietlicki, J. P. Putaud, Y. Balkanski, S. Fuzzi, J. Horth, G. K. Moortgat, R. Winterhalter, C. E. L. Myhre, K. Tsigaridis, E. Vignati, E. G. Stephanou and J. Wilson, Organic aerosol and global climate modelling: a review, *Atmos. Chem. Phys.*, 2005, **5**, 1053–1123.

6 E. von Schneidemesser, P. S. Monks, J. D. Allan, L. Bruhwiler, P. Forster, D. Fowler, A. Lauer, W. T. Morgan, P. Paasonen, M. Righi, K. Sindelarova and M. A. Sutton, Chemistry and the Linkages between Air Quality and Climate Change, *Chem. Rev.*, 2015, **115**, 3856–3897.

7 R. Atkinson, Atmospheric chemistry of VOCs and NOV, *Atmos. Environ.*, 2000, **34**, 2063–2101.

8 R. Atkinson and J. Arey, Gas-phase tropospheric chemistry of biogenic volatile organic compounds: a review, *Atmos. Environ.*, 2003, **37**, 197–219.

9 J. Lelieveld, T. M. Butler, J. N. Crowley, T. J. Dillon, H. Fischer, L. Ganzeveld, H. Harder, M. G. Lawrence, M. Martinez, D. Taraborrelli and J. Williams, Atmospheric oxidation capacity sustained by a tropical forest, *Nature*, 2008, **452**, 737–740.

10 L. K. Whalley, P. M. Edwards, K. L. Furneaux, A. Goddard, T. Ingham, M. J. Evans, D. Stone, J. R. Hopkins, C. E. Jones, A. Karunaharan, J. D. Lee, A. C. Lewis, P. S. Monks, S. J. Moller and D. E. Heard, Quantifying the magnitude of a missing hydroxyl radical source in a tropical rainforest, *Atmos. Chem. Phys.*, 2011, **11**, 7223–7233.

11 J. F. Pankow, An absorption model of gas/particle partitioning of organic compounds in the atmosphere, *Atmos. Environ.*, 1994, **28**, 185–188.

12 K. Lehtipalo, C. Yan, L. Dada, F. Bianchi, M. Xiao, R. Wagner, D. Stolzenburg, L. R. Ahonen, A. Amorim, A. Baccarini, P. S. Bauer, B. Baumgartner, A. Bergen, A.-K. Bernhammer, M. Breitenlechner, S. Brilke, A. Buchholz, S. B. Mazon, D. Chen, X. Chen, A. Dias, J. Dommen, D. C. Draper, J. Duplissy, M. Ehn, H. Finkenzeller, L. Fischer, C. Frege, C. Fuchs, O. Garmash, H. Gordon, J. Hakala, X. He, L. Heikkinen, M. Heinritzi, J. C. Helm, V. Hofbauer, C. R. Hoyle, T. Jokinen, J. Kangasluoma, V.-M. Kerminen, C. Kim, J. Kirkby, J. Kontkanen, A. Kürten, M. J. Lawler, H. Mai, S. Mathot, R. L. Mauldin, U. Molteni, L. Nichman, W. Nie, T. Nieminen, A. Ojdanic, A. Onnela, M. Passananti, T. Petäjä, F. Piel, V. Pospisilova, L. L. J. Quéléver, M. P. Rissanen, C. Rose, N. Sarnela, S. Schallhart, S. Schuchmann, K. Sengupta, M. Simon, M. Sipilä, C. Tauber, A. Tomé, J. Tröstl, O. Väisänen, A. L. Vogel, R. Volkamer, A. C. Wagner, M. Wang, L. Weitz,

D. Wimmer, P. Ye, A. Ylisirniö, Q. Zha, K. S. Carslaw, J. Curtius, N. M. Donahue, R. C. Flagan, A. Hansel, I. Riipinen, A. Virtanen, P. M. Winkler, U. Baltensperger, M. Kulmala and D. R. Worsnop, Multicomponent new particle formation from sulfuric acid, ammonia, and biogenic vapors, *Sci. Adv.*, 2018, **4**, eaau5363.

13 I. Riipinen, J. R. Pierce, T. Yli-Juuti, T. Nieminen, S. Häkkinen, M. Ehn, H. Junninen, K. Lehtipalo, T. Petäjä, J. Slowik, R. Chang, N. C. Shantz, J. Abbatt, W. R. Leaitch, V.-M. Kerminen, D. R. Worsnop, S. N. Pandis, N. M. Donahue and M. Kulmala, Organic condensation: a vital link connecting aerosol formation to cloud condensation nuclei (CCN) concentrations, *Atmos. Chem. Phys.*, 2011, **11**, 3865–3878.

14 J. Kirkby, J. Duplissy, K. Sengupta, C. Frege, H. Gordon, C. Williamson, M. Heinritzi, M. Simon, C. Yan, J. Almeida, J. Tröstl, T. Nieminen, I. K. Ortega, R. Wagner, A. Adamov, A. Amorim, A.-K. Bernhammer, F. Bianchi, M. Breitenlechner, S. Brilke, X. Chen, J. Craven, A. Dias, S. Ehrhart, R. C. Flagan, A. Franchin, C. Fuchs, R. Guida, J. Hakala, C. R. Hoyle, T. Jokinen, H. Junninen, J. Kangasluoma, J. Kim, M. Krapf, A. Kürten, A. Laaksonen, K. Lehtipalo, V. Makhmutov, S. Mathot, U. Molteni, A. Onnela, O. Peräkylä, F. Piel, T. Petäjä, A. P. Praplan, K. Pringle, A. Rap, N. A. D. Richards, I. Riipinen, M. P. Rissanen, L. Rondo, N. Sarnela, S. Schobesberger, C. E. Scott, J. H. Seinfeld, M. Sipilä, G. Steiner, Y. Stozhkov, F. Stratmann, A. Tomé, A. Virtanen, A. L. Vogel, A. C. Wagner, P. E. Wagner, E. Weingartner, D. Wimmer, P. M. Winkler, P. Ye, X. Zhang, A. Hansel, J. Dommen, N. M. Donahue, D. R. Worsnop, U. Baltensperger, M. Kulmala, K. S. Carslaw and J. Curtius, Ion-induced nucleation of pure biogenic particles, *Nature*, 2016, **533**, 521–526.

15 F. Riccobono, S. Schobesberger, C. Scott, J. Dommen, I. Ortega, L. Rondo, J. Almeida, A. Amorim, F. Bianchi, M. Breitenlechner, A. David, A. Downard, E. Dunne, J. Duplissy, S. Ehrhart, R. Flagan, A. Franchin, A. Hansel, H. Junninen, M. Kajos, H. Keskinen, A. Kupc, A. Kürten, A. Kvashin, A. Laaksonen, K. Lehtipalo, V. Makhmutov, S. Mathot, T. Nieminen, A. Onnela, T. Petäjä, A. Praplan, F. Santos, S. Schallhart, J. Seinfeld, M. Sipilä, D. Spracklen, Y. Stozhkov, F. Stratmann, A. Tomé, G. Tsagkogeorgas, P. Vaattovaara, Y. Viisanen, A. Vrtala, P. Wagner, E. Weingartner, H. Wex, D. Wimmer, K. Carslaw, J. Curtius, N. Donahue, J. Kirkby, M. Kulmala, D. Worsnop and U. Baltensperger, Oxidation products of biogenic emissions contribute to nucleation of atmospheric particles, *Science*, 2014, **344**, 717–721.

16 F. Bianchi, J. Tröstl, H. Junninen, C. Frege, S. Henne, C. R. Hoyle, U. Molteni, E. Herrmann, A. Adamov, N. Bukowiecki, X. Chen, J. Duplissy, M. Gysel, M. Hutterli, J. Kangasluoma, J. Kontkanen, A. Kürten, H. E. Manninen, S. Münch, O. Peräkylä, T. Petäjä, L. Rondo, C. Williamson, E. Weingartner, J. Curtius, D. R. Worsnop, M. Kulmala, J. Dommen and U. Baltensperger, New particle formation in the free troposphere: A question of chemistry and timing, *Science*, 2016, **352**, 1109–1112.

17 J. Tröstl, W. K. Chuang, H. Gordon, M. Heinritzi, C. Yan, U. Molteni, L. Ahlm, C. Frege, F. Bianchi, R. Wagner, M. Simon, K. Lehtipalo, C. Williamson, J. S. Craven, J. Duplissy, A. Adamov, J. Almeida, A.-K. Bernhammer, M. Breitenlechner, S. Brilke, A. Dias, S. Ehrhart, R. C. Flagan, A. Franchin, C. Fuchs, R. Guida, M. Gysel, A. Hansel, C. R. Hoyle, T. Jokinen, H. Junninen, J. Kangasluoma, H. Keskinen, J. Kim, M. Krapf, A. Kürten, A. Laaksonen, M. Lawler, M. Leiminger, S. Mathot, O. Möhler, T. Nieminen, A. Onnela, T. Petäjä, F. M. Piel, P. Miettinen, M. P. Rissanen, L. Rondo, N. Sarnela, S. Schobesberger, K. Sengupta, M. Sipilä, J. N. Smith, G. Steiner, A. Tomè, A. Virtanen, A. C. Wagner, E. Weingartner, D. Wimmer, P. M. Winkler, P. Ye, K. S. Carslaw, J. Curtius, J. Dommen, J. Kirkby, M. Kulmala, I. Riipinen, D. R. Worsnop, N. M. Donahue and U. Baltensperger, The role of low-volatility organic compounds in initial particle growth in the atmosphere, *Nature*, 2016, **533**, 527–531.

18 A. M. Dunker, B. Koo and G. Yarwood, Ozone sensitivity to isoprene chemistry and emissions and anthropogenic emissions in central California, *Atmos. Environ.*, 2016, **145**, 326–337.

19 M. Trainer, E. J. Williams, D. D. Parrish, M. P. Buhr, E. J. Allwine, H. H. Westberg, F. C. Fehsenfeld and S. C. Liu, Models and observations of the impact of natural hydrocarbons on rural ozone, *Nature*, 1987, **329**, 705–707.

20 W. L. Chameides, R. W. Lindsay, J. Richardson and C. S. Kiang, The Role of Biogenic Hydrocarbons in Urban Photochemical Smog: Atlanta as a Case Study, *Science*, 1988, **241**, 1473–1475.

21 N. R. Council, *Rethinking the Ozone Problem in Urban and Regional Air Pollution*, The National Academies Press, Washington, DC, 1991.

22 N. L. Ng, S. S. Brown, A. T. Archibald, E. Atlas, R. C. Cohen, J. N. Crowley, D. A. Day, N. M. Donahue, J. L. Fry, H. Fuchs, R. J. Griffin, M. I. Guzman, H. Herrmann, A. Hodzic, Y. Iinuma, J. L. Jimenez, A. Kiendler-Scharr, B. H. Lee, D. J. Luecken, J. Mao, R. McLaren, A. Mutzel, H. D. Osthoff, B. Ouyang, B. Picquet-Varrault, U. Platt, H. O. T. Pye, Y. Rudich, R. H. Schwantes, M. Shiraiwa, J. Stutz, J. A. Thornton, A. Tilgner, B. J. Williams and R. A. Zaveri, Nitrate radicals and biogenic volatile organic compounds: oxidation, mechanisms, and organic aerosol, *Atmos. Chem. Phys.*, 2017, **17**, 2103–2162.

23 A. Zare, P. S. Romer, T. Nguyen, F. N. Keutsch, K. Skog and R. C. Cohen, A comprehensive organic nitrate chemistry: insights into the lifetime of atmospheric organic nitrates, *Atmos. Chem. Phys.*, 2018, **18**, 15419–15436.

24 T. Berndt, S. Richters, T. Jokinen, N. Hyttinen, T. Kurtén, R. V. Otkjær, H. G. Kjaergaard, F. Stratmann, H. Herrmann, M. Sipilä, M. Kulmala and M. Ehn, Hydroxyl radical-induced formation of highly oxidized organic compounds, *Nat. Commun.*, 2016, **7**, 13677.

25 T. Jokinen, T. Berndt, R. Makkonen, V.-M. Kerminen, H. Junninen, P. Paasonen, F. Stratmann, H. Herrmann, A. B. Guenther, D. R. Worsnop, M. Kulmala, M. Ehn and M. Sipilä, Production of extremely low volatile organic compounds from biogenic emissions: Measured yields and atmospheric implications, *Proc. Natl. Acad. Sci. U. S. A.*, 2015, **112**, 7123–7128.

26 A. B. Guenther, X. Jiang, C. L. Heald, T. Sakulyanontvittaya, T. Duhl, L. K. Emmons and X. Wang, The Model of Emissions of Gases and Aerosols from Nature version 2.1 (MEGAN2.1): an extended and updated framework for modeling biogenic emissions, *Geosci. Model Dev.*, 2012, **5**, 1471–1492.

27 J. Peeters, T. L. Nguyen and L. Vereecken, HOx radical regeneration in the oxidation of isoprene, *Phys. Chem. Chem. Phys.*, 2009, **11**, 5935–5939.

28 X. Ren, J. R. Olson, J. H. Crawford, W. H. Brune, J. Mao, R. B. Long, Z. Chen, G. Chen, M. A. Avery, G. W. Sachse, J. D. Barrick, G. S. Diskin, L. G. Huey, A. Fried, R. C. Cohen, B. Heikes, P. O. Wennberg, H. B. Singh, D. R. Blake and R. E. Shetter, HOx chemistry during INTEX-A 2004: Observation, model calculation, and comparison with previous studies, *J. Geophys. Res.: Atmos.*, 2008, **113**, D05310.

29 D. Taraborrelli, M. G. Lawrence, T. M. Butler, R. Sander and J. Lelieveld, Mainz Isoprene Mechanism 2 (MIM2): an isoprene oxidation mechanism for regional and global atmospheric modelling, *Atmos. Chem. Phys.*, 2009, **9**, 2751–2777.

30 P. O. Wennberg, K. H. Bates, J. D. Crounse, L. G. Dodson, R. C. McVay, L. A. Mertens, T. B. Nguyen, E. Praske, R. H. Schwantes, M. D. Smarte, J. M. St Clair, A. P. Teng, X. Zhang and J. H. Seinfeld, Gas-Phase Reactions of Isoprene and Its Major Oxidation Products, *Chem. Rev.*, 2018, **118**, 3337–3390.

31 M. A. H. Khan, M. E. Jenkin, A. Foulds, R. G. Derwent, C. J. Percival and D. E. Shallcross, A modeling study of secondary organic aerosol formation from sesquiterpenes using the STOCHEM global chemistry and transport model: SOA FORMATION FROM SESQUITERPENES, *J. Geophys. Res.: Atmos.*, 2017, **122**, 4426–4439.

32 R. Baraldi, C. Chieco, L. Neri, O. Facini, F. Rapparini, L. Morrone, A. Rotondi and G. Carriero, An integrated study on air mitigation potential of urban vegetation: From a multi-trait approach to modeling, *Urban For. Urban Green.*, 2019, **41**, 127–138.

33 W. P. L. Carter, *Updated Maximum Incremental Reactivity Scale and Hydrocarbon Bin Reactivities for Regulatory Applications (California Air Resources Board Contract 07-339)*, College of Engineering Center for Environmental Research and Technology University of California, Riverside, CA, 2010.

34 S. Gu, A. Guenther and C. Faiola, Effects of Anthropogenic and Biogenic Volatile Organic Compounds on Los Angeles Air Quality, *Environ. Sci. Technol.*, 2021, **55**, 12191–12201.

35 M. L. Luttkus, R. Wolke, B. Heinold, A. Tilgner, L. Poulain and H. Herrmann, in *Air Pollution Modeling and its Application XXVII*, ed. C. Mensink and V. Matthias, Springer Berlin Heidelberg, Berlin, Heidelberg, 2021, pp. 11–17.

36 H. Li, M. R. Canagaratna, M. Riva, P. Rantala, Y. Zhang, S. Thomas, L. Heikkinen, P.-M. Flaud, E. Villenave, E. Perraudin, D. Worsnop, M. Kulmala, M. Ehn and F. Bianchi, Atmospheric organic vapors in two European pine forests measured by a Vocus PTR-TOF: insights into monoterpene and sesquiterpene oxidation processes, *Atmos. Chem. Phys.*, 2021, **21**, 4123–4147.

37 W. R. Stockwell, F. Kirchner, M. Kuhn and S. Seefeld, A new mechanism for regional atmospheric chemistry modeling, *J. Geophys. Res.*, 1997, **102**, 25847–25879.

38 W. S. Goliff, W. R. Stockwell and C. V. Lawson, The regional atmospheric chemistry mechanism, version 2, *Atmos. Environ.*, 2013, **68**, 174–185.

39 M. G. Schultz, S. Stadtler, S. Schröder, D. Taraborrelli, B. Franco, J. Krefting, A. Henrot, S. Ferrachat, U. Lohmann, D. Neubauer, C. Siegenthaler-Le Drian, S. Wahl, H. Kokkola, T. Kühn, S. Rast, H. Schmidt, P. Stier, D. Kinnison, G. S. Tyndall, J. J. Orlando and C. Wespes, The chemistry–climate model ECHAM6.3-HAM2.3-MOZ1.0, *Geosci. Model Dev.*, 2018, **11**, 1695–1723.

40 L. K. Emmons, S. Walters, P. G. Hess, J.-F. Lamarque, G. G. Pfister, D. Fillmore, C. Granier, A. Guenther, D. Kinnison, T. Laepple, J. Orlando, X. Tie, G. Tyndall, C. Wiedinmyer, S. L. Baughcum and S. Kloster, Description and evaluation of the Model for Ozone and Related chemical Tracers, version 4 (MOZART-4), *Geosci. Model Dev.*, 2010, **3**, 43–67.

41 G. Yarwood, Y. Shi and R. Beardsley, *Develop CB7 Chemical Mechanism for CAMx Ozone Modeling, Final Rep.*, 2021, 582-21-21802-020.

42 W. P. L. Carter, Development of the SAPRC-07 chemical mechanism, *Atmos. Environ.*, 2010, **44**, 5324–5335.

43 W. P. L. Carter, *Documentation of the SAPRC-18 Mechanism (Report to California Air Resources Board Contract No 11-761)*, College of Engineering Center for Environmental Research and Technology University of California, Riverside, CA, 2020.

44 A. Mutzel, Y. Zhang, O. Böge, M. Rodigast, A. Kolodziejczyk, X. Wang and H. Herrmann, Importance of secondary organic aerosol formation of α-pinene, limonene, and *m*-cresol comparing day- and nighttime radical chemistry, *Atmos. Chem. Phys.*, 2021, **21**, 8479–8498.

45 J. H. Seinfeld, G. B. Erdakos, W. E. Asher and J. F. Pankow, Modeling the Formation of Secondary Organic Aerosol (SOA). 2. The Predicted Effects of Relative Humidity on Aerosol Formation in the α-Pinene-, β-Pinene-, Sabinene-, Δ^3-Carene-, and Cyclohexene-Ozone Systems, *Environ. Sci. Technol.*, 2001, **35**, 1806–1817.

46 J. F. Pankow, J. H. Seinfeld, W. E. Asher and G. B. Erdakos, Modeling the Formation of Secondary Organic Aerosol. 1. Application of Theoretical Principles to Measurements Obtained in the α-Pinene/, β-Pinene/, Sabinene/, Δ^3-Carene/, and Cyclohexene/Ozone Systems, *Environ. Sci. Technol.*, 2001, **35**, 1164–1172.

47 D. Thomsen, J. Elm, B. Rosati, J. T. Skønager, M. Bilde and M. Glasius, Large Discrepancy in the Formation of Secondary Organic Aerosols from Structurally Similar Monoterpenes, *ACS Earth Space Chem.*, 2021, **5**, 632–644.
48 C. J. Colville and R. J. Griffin, The roles of individual oxidants in secondary organic aerosol formation from Δ3-carene: 2. soa formation and oxidant contribution, *Atmos. Environ.*, 2004, **38**, 4013–4023.
49 J. D. Blande, J. K. Holopainen and Ü. Niinemets, Plant volatiles in polluted atmospheres: stress responses and signal degradation: Plant volatiles in a polluted atmosphere, *Plant, Cell Environ.*, 2014, **37**, 1892–1904.
50 J. K. Holopainen and J. Gershenzon, Multiple stress factors and the emission of plant VOCs, *Trends Plant Sci.*, 2010, **15**, 176–184.
51 Ü. Niinemets, Mild versus severe stress and BVOCs: thresholds, priming and consequences, *Trends Plant Sci.*, 2009, **15**, 145–153.
52 Ü. Niinemets, A. Arneth, U. Kuhn, R. K. Monson, J. Peñuelas and M. Staudt, The emission factor of volatile isoprenoids: stress, acclimation, and developmental responses, *Biogeosciences*, 2010, **7**, 2203–2223.
53 R. Grote, M. Sharma, A. Ghirardo and J.-P. Schnitzler, A New Modeling Approach for Estimating Abiotic and Biotic Stress-Induced de novo Emissions of Biogenic Volatile Organic Compounds From Plants, *Front. For. Glob. Change*, 2019, **2**, 26.
54 C. Bloss, V. Wagner, M. E. Jenkin, R. Volkamer, W. J. Bloss, J. D. Lee, D. E. Heard, K. Wirtz, M. Martin-Reviejo, G. Rea, J. C. Wenger and M. J. Pilling, Development of a detailed chemical mechanism (MCMv3.1) for the atmospheric oxidation of aromatic hydrocarbons, *Atmos. Chem. Phys.*, 2005, **5**, 641–664.
55 M. E. Jenkin, S. M. Saunders and M. J. Pilling, The tropospheric degradation of volatile organic compounds: a protocol for mechanism development, *Atmos. Environ.*, 1997, **31**, 81–104.
56 M. E. Jenkin, S. M. Saunders, V. Wagner and M. J. Pilling, Protocol for the development of the Master Chemical Mechanism, MCM v3 (Part B): tropospheric degradation of aromatic volatile organic compounds, *Atmos. Chem. Phys.*, 2003, **3**, 181–193.
57 M. E. Jenkin, K. P. Wyche, C. J. Evans, T. Carr, P. S. Monks, M. R. Alfarra, M. H. Barley, G. B. McFiggans, J. C. Young and A. R. Rickard, Development and chamber evaluation of the MCM v3.2 degradation scheme for β-caryophyllene, *Atmos. Chem. Phys.*, 2012, **12**, 5275–5308.
58 M. E. Jenkin, J. C. Young and A. R. Rickard, The MCM v3.3.1 degradation scheme for isoprene, *Atmos. Chem. Phys.*, 2015, **15**, 11433–11459.
59 S. M. Saunders, M. E. Jenkin, R. G. Derwent and M. J. Pilling, Protocol for the development of the Master Chemical Mechanism, MCM v3 (Part A): tropospheric degradation of non-aromatic volatile organic compounds, *Atmos. Chem. Phys.*, 2003, **3**, 161–180.
60 D. E. Kinnison, G. P. Brasseur, S. Walters, R. R. Garcia, D. R. Marsh, F. Sassi, V. L. Harvey, C. E. Randall, L. Emmons, J. F. Lamarque, P. Hess, J. J. Orlando, X. X. Tie, W. Randel, L. L. Pan, A. Gettelman, C. Granier, T. Diehl, U. Niemeier and A. J. Simmons, Sensitivity of chemical tracers to meteorological parameters in the MOZART-3 chemical transport model, *J. Geophys. Res.: Atmos.*, 2007, **112**, D20302.
61 F. Paulot, J. D. Crounse, H. G. Kjaergaard, A. Kürten, J. M. S. Clair, J. H. Seinfeld and P. O. Wennberg, Unexpected Epoxide Formation in the Gas-Phase Photooxidation of Isoprene, *Science*, 2009, **325**, 730–733.
62 G. M. Wolfe, J. D. Crounse, J. D. Parrish, J. M. St. Clair, M. R. Beaver, F. Paulot, T. P. Yoon, P. O. Wennberg and F. N. Keutsch, Photolysis, OH reactivity and ozone reactivity of a proxy for isoprene-derived hydroperoxyenals (HPALDs), *Phys. Chem. Chem. Phys.*, 2012, **14**, 7276–7286.
63 M. Karl, H.-P. Dorn, F. Holland, R. Koppmann, D. Poppe, L. Rupp, A. Schaub and A. Wahner, Product study of the reaction of OH radicals with isoprene in the atmosphere simulation chamber SAPHIR, *J. Atmos. Chem.*, 2006, **55**, 167–187.
64 R. Wolke, W. Schröder, R. Schrödner and E. Renner, Influence of grid resolution and meteorological forcing on simulated European air quality: A sensitivity study with the modeling system COSMO–MUSCAT, *Atmos. Environ.*, 2012, **53**, 110–130.
65 R. Stern, P. Builtjes, M. Schaap, R. Timmermans, R. Vautard, A. Hodzic, M. Memmesheimer, H. Feldmann, E. Renner, R. Wolke and A. Kerschbaumer, A model inter-comparison study focussing on episodes with elevated PM10 concentrations, *Atmos. Environ.*, 2008, **42**, 4567–4588.
66 E. Renner and R. Wolke, Modelling the formation and atmospheric transport of secondary inorganic aerosols with special attention to regions with high ammonia emissions, *Atmos. Environ.*, 2010, **44**, 1904–1912.
67 R. Atkinson, D. L. Baulch, R. A. Cox, J. N. Crowley, R. F. Hampson, R. G. Hynes, M. E. Jenkin, M. J. Rossi and J. Troe, Evaluated kinetic and photochemical data for atmospheric chemistry: Volume I - gas phase reactions of O_x, HO_x, NO_x and SO_x species, *Atmos. Chem. Phys.*, 2004, **4**, 1461–1738.
68 R. Atkinson, D. L. Baulch, R. A. Cox, J. N. Crowley, R. F. Hampson, R. G. Hynes, M. E. Jenkin, M. J. Rossi, J. Troe and I. Subcommittee, Evaluated kinetic and photochemical data for atmospheric chemistry: Volume II – gas phase reactions of organic species, *Atmos. Chem. Phys.*, 2006, **6**, 3625–4055.
69 R. Atkinson, D. L. Baulch, R. A. Cox, J. N. Crowley, R. F. Hampson, R. G. Hynes, M. E. Jenkin, M. J. Rossi and J. Troe, Evaluated kinetic and photochemical data for atmospheric chemistry: Volume III – gas phase reactions of inorganic halogens, *Atmos. Chem. Phys.*, 2007, **7**, 981–1191.
70 R. Atkinson, D. L. Baulch, R. A. Cox, J. N. Crowley, R. F. Hampson, R. G. Hynes, M. E. Jenkin, M. J. Rossi, J. Troe and T. J. Wallington, Evaluated kinetic and photochemical data for atmospheric chemistry: Volume

IV – gas phase reactions of organic halogen species, *Atmos. Chem. Phys.*, 2008, **8**, 4141–4496.

71 J. N. Crowley, M. Ammann, R. A. Cox, R. G. Hynes, M. E. Jenkin, A. Mellouki, M. J. Rossi, J. Troe and T. J. Wallington, Evaluated kinetic and photochemical data for atmospheric chemistry: Volume V – heterogeneous reactions on solid substrates, *Atmos. Chem. Phys.*, 2010, **10**, 9059–9223.

72 M. Ammann, R. A. Cox, J. N. Crowley, M. E. Jenkin, A. Mellouki, M. J. Rossi, J. Troe and T. J. Wallington, Evaluated kinetic and photochemical data for atmospheric chemistry: Volume VI – heterogeneous reactions with liquid substrates, *Atmos. Chem. Phys.*, 2013, **13**, 8045–8228.

73 R. A. Cox, M. Ammann, J. N. Crowley, H. Herrmann, M. E. Jenkin, V. F. McNeill, A. Mellouki, J. Troe and T. J. Wallington, Evaluated kinetic and photochemical data for atmospheric chemistry: Volume VII – Criegee intermediates, *Atmos. Chem. Phys.*, 2020, **20**, 13497–13519.

74 A. Mellouki, M. Ammann, R. A. Cox, J. N. Crowley, H. Herrmann, M. E. Jenkin, V. F. McNeill, J. Troe and T. J. Wallington, Evaluated kinetic and photochemical data for atmospheric chemistry: volume VIII – gas-phase reactions of organic species with four, or more, carbon atoms ($\geq C_4$), *Atmos. Chem. Phys.*, 2021, **21**, 4797–4808.

75 M. E. Jenkin, R. Valorso, B. Aumont, A. R. Rickard and T. J. Wallington, Estimation of rate coefficients and branching ratios for gas-phase reactions of OH with aliphatic organic compounds for use in automated mechanism construction, *Atmos. Chem. Phys.*, 2018, **18**, 9297–9328.

76 J.-F. Müller, T. Stavrakou and J. Peeters, Chemistry and deposition in the Model of Atmospheric composition at Global and Regional scales using Inversion Techniques for Trace gas Emissions (MAGRITTE v1.1) – Part 1: Chemical mechanism, *Geosci. Model Dev.*, 2019, **12**, 2307–2356.

77 H. Hou, B. Wang and Y. Gu, Mechanism of the OH+CH2CO reaction, *Phys. Chem. Chem. Phys.*, 2000, **2**, 2329–2334.

78 L. Sheps, B. Rotavera, A. J. Eskola, D. L. Osborn, C. A. Taatjes, K. Au, D. E. Shallcross, M. A. H. Khan and C. J. Percival, The reaction of Criegee intermediate CH_2OO with water dimer: primary products and atmospheric impact, *Phys. Chem. Chem. Phys.*, 2017, **19**, 21970–21979.

79 T. B. Nguyen, G. S. Tyndall, J. D. Crounse, A. P. Teng, K. H. Bates, R. H. Schwantes, M. M. Coggon, L. Zhang, P. Feiner, D. O. Milller, K. M. Skog, J. C. Rivera-Rios, M. Dorris, K. F. Olson, A. Koss, R. J. Wild, S. S. Brown, A. H. Goldstein, J. A. de Gouw, W. H. Brune, F. N. Keutsch, J. H. Seinfeld and P. O. Wennberg, Atmospheric fates of Criegee intermediates in the ozonolysis of isoprene, *Phys. Chem. Chem. Phys.*, 2016, **18**, 10241–10254.

80 B. Franco, T. Blumenstock, C. Cho, L. Clarisse, C. Clerbaux, P.-F. Coheur, M. De Mazière, I. De Smedt, H.-P. Dorn, T. Emmerichs, H. Fuchs, G. Gkatzelis, D. W. T. Griffith, S. Gromov, J. W. Hannigan, F. Hase, T. Hohaus, N. Jones, A. Kerkweg, A. Kiendler-Scharr, E. Lutsch, E. Mahieu, A. Novelli, I. Ortega, C. Paton-Walsh, M. Pommier, A. Pozzer, D. Reimer, S. Rosanka, R. Sander, M. Schneider, K. Strong, R. Tillmann, M. Van Roozendael, L. Vereecken, C. Vigouroux, A. Wahner and D. Taraborrelli, Ubiquitous atmospheric production of organic acids mediated by cloud droplets, *Nature*, 2021, **593**, 233–237.

81 D. B. Millet, M. Baasandorj, D. K. Farmer, J. A. Thornton, K. Baumann, P. Brophy, S. Chaliyakunnel, J. A. de Gouw, M. Graus, L. Hu, A. Koss, B. H. Lee, F. D. Lopez-Hilfiker, J. A. Neuman, F. Paulot, J. Peischl, I. B. Pollack, T. B. Ryerson, C. Warneke, B. J. Williams and J. Xu, A large and ubiquitous source of atmospheric formic acid, *Atmos. Chem. Phys.*, 2015, **15**, 6283–6304.

82 B. Yuan, P. R. Veres, C. Warneke, J. M. Roberts, J. B. Gilman, A. Koss, P. M. Edwards, M. Graus, W. C. Kuster, S.-M. Li, R. J. Wild, S. S. Brown, W. P. Dubé, B. M. Lerner, E. J. Williams, J. E. Johnson, P. K. Quinn, T. S. Bates, B. Lefer, P. L. Hayes, J. L. Jimenez, R. J. Weber, R. Zamora, B. Ervens, D. B. Millet, B. Rappenglück and J. A. de Gouw, Investigation of secondary formation of formic acid: urban environment vs. oil and gas producing region, *Atmos. Chem. Phys.*, 2015, **15**, 1975–1993.

83 L. Chen, Y. Huang, Y. Xue, Z. Jia and W. Wang, OH-initiated atmospheric degradation of hydroxyalkyl hydroperoxides: mechanism, kinetics, and structure–activity relationship, *Atmos. Chem. Phys.*, 2022, **22**, 3693–3711.

84 M. E. Jenkin, M. D. Hurley and T. J. Wallington, Investigation of the radical product channel of the CH3C(O)O2 + HO2 reaction in the gas phase, *Phys. Chem. Chem. Phys.*, 2007, **9**, 3149–3162.

85 M. E. Jenkin, R. Valorso, B. Aumont and A. R. Rickard, Estimation of rate coefficients and branching ratios for reactions of organic peroxy radicals for use in automated mechanism construction, *Atmos. Chem. Phys.*, 2019, **19**, 7691–7717.

86 K. H. Bates, D. J. Jacob, K. Li, P. D. Ivatt, M. J. Evans, Y. Yan and J. Lin, Development and evaluation of a new compact mechanism for aromatic oxidation in atmospheric models, *Atmos. Chem. Phys.*, 2021, **21**, 18351–18374.

87 L. Vereecken, P. T. M. Carlsson, A. Novelli, F. Bernard, S. S. Brown, C. Cho, J. N. Crowley, H. Fuchs, W. Mellouki, D. Reimer, J. Shenolikar, R. Tillmann, L. Zhou, A. Kiendler-Scharr and A. Wahner, Theoretical and experimental study of peroxy and alkoxy radicals in the NO_3-initiated oxidation of isoprene, *Phys. Chem. Chem. Phys.*, 2021, **23**, 5496–5515.

88 J. H. Seinfeld and S. N. Pandis, *Atmospheric Chemistry and Physics: from Air Pollution to Climate Change*, J. Wiley, Hoboken, N.J, 2nd edn, 2006.

89 A. P. Teng, J. D. Crounse and P. O. Wennberg, Isoprene Peroxy Radical Dynamics, *J. Am. Chem. Soc.*, 2017, **139**, 5367–5377.

90 R. H. Schwantes, L. K. Emmons, J. J. Orlando, M. C. Barth, G. S. Tyndall, S. R. Hall, K. Ullmann, J. M. St. Clair, D. R. Blake, A. Wisthaler and T. P. V. Bui, Comprehensive

isoprene and terpene gas-phase chemistry improves simulated surface ozone in the southeastern US, *Atmos. Chem. Phys.*, 2020, **20**, 3739–3776.

91 R. Wolke, A. M. Sehili, M. Simmel, O. Knoth, A. Tilgner and H. Herrmann, SPACCIM: A parcel model with detailed microphysics and complex multiphase chemistry, *Atmos. Environ.*, 2005, **39**, 4375–4388.

92 R. Wolke, O. Knoth, O. Hellmuth, W. Schröder and E. Renner, in *Parallel Computing*, ed. G. R. Joubert, W. E. Nagel, F. J. Peters and W. V. Walter, North-Holland, 2004, vol. 13, pp. 363–369.

93 M. L. Bell, K. Ebisu and R. D. Peng, Community-level spatial heterogeneity of chemical constituent levels of fine particulates and implications for epidemiological research, *J. Exposure Sci. Environ. Epidemiol.*, 2011, **21**, 372–384.

94 R. Schrödner, A. Tilgner, R. Wolke and H. Herrmann, Modeling the multiphase processing of an urban and a rural air mass with COSMO–MUSCAT, *Urban Climate*, 2014, **10**, 720–731.

95 Y. Chen, R. Wolke, L. Ran, W. Birmili, G. Spindler, W. Schröder, H. Su, Y. Cheng, I. Tegen and A. Wiedensohler, A parameterization of the heterogeneous hydrolysis of N_2O_5 \hack\break for mass-based aerosol models: improvement of \hack\break particulate nitrate prediction, *Atmos. Chem. Phys.*, 2018, **18**, 673–689.

96 M. E. Jenkin, M. A. H. Khan, D. E. Shallcross, R. Bergström, D. Simpson, K. L. C. Murphy and A. R. Rickard, The CRI v2.2 reduced degradation scheme for isoprene, *Atmos. Environ.*, 2019, **212**, 172–182.

97 A. Guenther, C. N. Hewitt, D. Erickson, R. Fall, C. Geron, T. Graedel, P. Harley, L. Klinger, M. Lerdau, W. A. Mckay, T. Pierce, B. Scholes, R. Steinbrecher, R. Tallamraju, J. Taylor and P. Zimmerman, A global model of natural volatile organic compound emissions, *J. Geophys. Res.: Atmos.*, 1995, **100**, 8873–8892.

98 J. G. J. Olivier, A. F. Bouwman, C. W. M. Van derMaas, J. J. M. Berdowski, C. Veldt, J. P. J. Bloos, A. J. H. Visschedijk, P. Y. J. Zandveld and J. L. Haverlag, *Description of EDGAR Version 2.0. A Set of Global Emission Inventories of Greenhouse Gases and Ozone-Depleting Substances for All Anthropogenic and Most Natural Sources on a Per Country Basis and on 1degree X1degree Grid (RIVM Rapport 771060002*, RIVM, Bilthoven, Netherlands, 1996.

99 B. Ervens, CAPRAM 2.4 (MODAC mechanism): An extended and condensed tropospheric aqueous phase mechanism and its application, *J. Geophys. Res.*, 2003, **108**, 4426.

100 H. Herrmann, D. Hoffmann, T. Schaefer, P. Bräuer and A. Tilgner, Tropospheric Aqueous-Phase Free-Radical Chemistry: Radical Sources, Spectra, Reaction Kinetics and Prediction Tools, *ChemPhysChem*, 2010, **11**, 3796–3822.

101 E. H. Hoffmann, A. Tilgner, R. Wolke, O. Böge, A. Walter and H. Herrmann, Oxidation of substituted aromatic hydrocarbons in the tropospheric aqueous phase: kinetic mechanism development and modelling, *Phys. Chem. Chem. Phys.*, 2018, **20**, 10960–10977.

102 A. Tilgner, P. Bräuer, R. Wolke and H. Herrmann, Modelling multiphase chemistry in deliquescent aerosols and clouds using CAPRAM3.0i, *J. Atmos. Chem.*, 2013, **70**, 221–256.

103 A. Tilgner and H. Herrmann, Radical-driven carbonyl-to-acid conversion and acid degradation in tropospheric aqueous systems studied by CAPRAM, *Atmos. Environ.*, 2010, **44**, 5415–5422.

104 P. Middleton, W. R. Stockwell and W. P. L. Carter, Aggregation and analysis of volatile organic compound emissions for regional modeling, *Atmos. Environ., Part A*, 1990, **24**, 1107–1133.

105 U. Im, R. Bianconi, E. Solazzo, I. Kioutsioukis, A. Badia, A. Balzarini, R. Baró, R. Bellasio, D. Brunner, C. Chemel, G. Curci, J. Flemming, R. Forkel, L. Giordano, P. Jiménez-Guerrero, M. Hirtl, A. Hodzic, L. Honzak, O. Jorba, C. Knote, J. J. P. Kuenen, P. A. Makar, A. Manders-Groot, L. Neal, J. L. Pérez, G. Pirovano, G. Pouliot, R. S. Jose, N. Savage, W. Schroder, R. S. Sokhi, D. Syrakov, A. Torian, P. Tuccella, J. Werhahn, R. Wolke, K. Yahya, R. Zabkar, Y. Zhang, J. Zhang, C. Hogrefe and S. Galmarini, Evaluation of operational on-line-coupled regional air quality models over Europe and North America in the context of AQMEII phase 2. Part I: Ozone, *Atmos. Environ.*, 2015, **115**, 404–420.

106 U. Im, R. Bianconi, E. Solazzo, I. Kioutsioukis, A. Badia, A. Balzarini, R. Baró, R. Bellasio, D. Brunner, C. Chemel, G. Curci, H. D. van der Gon, J. Flemming, R. Forkel, L. Giordano, P. Jiménez-Guerrero, M. Hirtl, A. Hodzic, L. Honzak, O. Jorba, C. Knote, P. A. Makar, A. Manders-Groot, L. Neal, J. L. Pérez, G. Pirovano, G. Pouliot, R. S. Jose, N. Savage, W. Schroder, R. S. Sokhi, D. Syrakov, A. Torian, P. Tuccella, K. Wang, J. Werhahn, R. Wolke, R. Zabkar, Y. Zhang, J. Zhang, C. Hogrefe and S. Galmarini, Evaluation of operational online-coupled regional air quality models over Europe and North America in the context of AQMEII phase 2. Part II: Particulate matter, *Atmos. Environ.*, 2015, **115**, 421–441.

107 E. Solazzo, R. Bianconi, G. Pirovano, V. Matthias, R. Vautard, M. D. Moran, K. W. Appel, B. Bessagnet, J. Brandt, J. H. Christensen, C. Chemel, I. Coll, J. Ferreira, R. Forkel, X. V. Francis, G. Grell, P. Grossi, A. B. Hansen, A. I. Miranda, U. Nopmongcol, M. Prank, K. N. Sartelet, M. Schaap, J. D. Silver, R. S. Sokhi, J. Vira, J. Werhahn, R. Wolke, G. Yarwood, J. Zhang, S. T. Rao and S. Galmarini, Operational model evaluation for particulate matter in Europe and North America in the context of AQMEII, *Atmos. Environ.*, 2012, **53**, 75–92.

108 E. Solazzo, R. Bianconi, R. Vautard, K. W. Appel, M. D. Moran, C. Hogrefe, B. Bessagnet, J. Brandt, J. H. Christensen, C. Chemel, I. Coll, H. D. van der Gon, J. Ferreira, R. Forkel, X. V. Francis, G. Grell, P. Grossi, A. B. Hansen, A. Jeričević, L. Kraljević, A. I. Miranda, U. Nopmongcol, G. Pirovano, M. Prank, A. Riccio, K. N. Sartelet, M. Schaap, J. D. Silver, R. S. Sokhi, J. Vira, J. Werhahn, R. Wolke, G. Yarwood, J. Zhang, S. T. Rao and S. Galmarini, Model evaluation and ensemble

modelling of surface-level ozone in Europe and North America in the context of AQMEII, *Atmos. Environ.*, 2012, **53**, 60–74.

109 R. Steinbrecher, G. Smiatek, R. Köble, G. Seufert, J. Theloke, K. Hauff, P. Ciccioli, R. Vautard and G. Curci, Intra- and inter-annual variability of VOC emissions from natural and semi-natural vegetation in Europe and neighbouring countries, *Atmos. Environ.*, 2009, **43**, 1380–1391.

110 K. H. Schlünzen and S. Pahl, Modification of dry deposition in a developing sea-breeze circulation—A numerical case study, *Atmos. Environ., Part A*, 1992, **26**, 51–61.

111 K. H. Schlünzen, U. Bungert, D. D. Flagg, B. H. Fock, A. Gierisch, D. Grawe, P. Kirschner, C. Lüpkes, V. Reinhardt, H. Ries, R. Schoetter, C. Spensberger and M. Uphoff, *Technical Documentation of the Multiscale Model System M-SYS*.

112 K. H. Schlunzen and J. J. Katzfey, Relevance of sub-grid-scale land-use effects for mesoscale models, *Tellus A*, 2003, **55**, 232–246.

113 T. B. Nguyen, J. D. Crounse, A. P. Teng, J. M. St. Clair, F. Paulot, G. M. Wolfe and P. O. Wennberg, Rapid deposition of oxidized biogenic compounds to a temperate forest, *Proc. Natl. Acad. Sci. U. S. A.*, 2015, **112**, E392–E401.

114 T. Emmerichs, A. Kerkweg, H. Ouwersloot, S. Fares, I. Mammarella and D. Taraborrelli, A revised dry deposition scheme for land–atmosphere exchange of trace gases in ECHAM/MESSy v2.54, *Geosci. Model Dev.*, 2021, **14**, 495–519.

115 Z. Wu, L. Zhang, J. T. Walker, P. A. Makar, J. A. Perlinger and X. Wang, Extension of a gaseous dry deposition algorithm to oxidized volatile organic compounds and hydrogen cyanide for application in chemistry transport models, *Geosci. Model Dev.*, 2021, **14**, 5093–5105.

116 L. Zhang, J. R. Brook and R. Vet, A revised parameterization for gaseous dry deposition in air-quality models, *Atmos. Chem. Phys.*, 2003, **3**, 2067–2082.

117 D. Jeong, R. Seco, L. Emmons, R. Schwantes, Y. Liu, K. A. McKinney, S. T. Martin, F. N. Keutsch, D. Gu, A. B. Guenther, O. Vega, J. Tota, R. A. F. Souza, S. R. Springston, T. B. Watson and S. Kim, Reconciling Observed and Predicted Tropical Rainforest OH Concentrations, *J. Geophys. Res.: Atmos.*, 2022, **127**, e2020JD032901.

118 S. M. MacDonald, H. Oetjen, A. S. Mahajan, L. K. Whalley, P. M. Edwards, D. E. Heard, C. E. Jones and J. M. C. Plane, DOAS measurements of formaldehyde and glyoxal above a south-east Asian tropical rainforest, *Atmos. Chem. Phys.*, 2012, **12**, 5949–5962.

119 F. L. Eisele, D. J. Tanner, C. A. Cantrell and J. G. Calvert, Measurements and steady state calculations of OH concentrations at Mauna Loa Observatory, *J. Geophys. Res.: Atmos.*, 1996, **101**, 14665–14679.

120 F. Holland, A. Hofzumahaus, J. Schäfer, A. Kraus and H.-W. Pätz, Measurements of OH and HO2 radical concentrations and photolysis frequencies during BERLIOZ, *J. Geophys. Res.: Atmos.*, 2003, **108**, PHO 2-1–PHO 2-23.

121 V. Michoud, S. Sauvage, T. Léonardis, I. Fronval, A. Kukui, N. Locoge and S. Dusanter, Field measurements of methylglyoxal using proton transfer reaction time-of-flight mass spectrometry and comparison to the DNPH–HPLC–UV method, *Atmos. Meas. Tech.*, 2018, **11**, 5729–5740.